

A Hamiltonian Dysthe equation for hydroelastic waves in a compressed ice sheet

Philippe Guyenne¹, Adilbek Kairzhan^{2,†} and Catherine Sulem³

¹Department of Mathematical Sciences, University of Delaware, Newark, DE 19716, USA

²Department of Mathematics, Nazarbayev University, 010000, Kazakhstan

³Department of Mathematics, University of Toronto, Ontario M5S2E4, Canada

(Received 18 September 2024; revised 21 November 2024; accepted 25 November 2024)

Nonlinear hydroelastic waves along a compressed ice sheet lying on top of a two-dimensional fluid of infinite depth are investigated. Based on a Hamiltonian formulation of this problem and by applying techniques from Hamiltonian perturbation theory, a Hamiltonian Dysthe equation is derived for the slowly varying envelope of modulated wavetrains. This derivation is further complicated here by the presence of cubic resonances for which a detailed analysis is given. A Birkhoff normal form transformation is introduced to eliminate non-resonant triads while accommodating resonant ones. It also provides a non-perturbative scheme to reconstruct the ice-sheet deformation from the wave envelope. Linear predictions on the modulational instability of Stokes waves in sea ice are established, and implications for the existence of solitary wave packets are discussed for a range of values of ice compression relative to ice bending. This Dysthe equation is solved numerically to test these predictions. Its numerical solutions are compared with direct simulations of the full Euler system, and very good agreement is observed.

Key words: Hamiltonian theory, elastic waves, surface gravity waves

1. Introduction

This paper is devoted to the study of hydroelastic waves describing the deformations of an ice sheet floating on water, a problem of importance in the polar regions. It is part of a large class of hydroelasticity problems concerning the interaction between deformable bodies and a surrounding fluid, and it has many engineering and industrial applications. A major challenge concerns modelling the mutual interactions between sea ice and water waves. On one hand, the presence of sea ice affects the wave dynamics in various different ways.

† Email address for correspondence: akairzhan@nu.edu.kz

On the other hand, waves can deform the sea ice, move it vertically and horizontally, and possibly break it up. There is a large literature on linear models, valid for small-amplitude waves and small ice deflections, which have focused on quantifying wave attenuation due to sea ice via scattering or other dissipative processes (Chen, Gilbert & Guyenne 2019; Squire 2020). In this framework, a multitude of configurations have been considered, including a continuous ice cover or a fragmented ice cover made of multiple discrete floes with possibly different characteristics.

However, intense wave-in-ice events have been reported and their analysis suggests that linear theory is not sufficient to explain these observations (Marko 2003). It is also expected that, in the context of climate change, the proliferation of open water (or more compliant sea ice) in the polar regions will promote wave growth with larger amplitudes and stronger nonlinear effects. Motivated in part by these considerations, nonlinear theory has drawn increasing attention in recent years, with an emphasis on describing nonlinear ice deformations subject to water wave excitation. Such studies have typically represented the ice cover as a continuous elastic plate of infinite extent, with various effects depending on the complexity of the elasticity model. Their results range from direct numerical simulations of the full nonlinear equations to weakly nonlinear predictions in asymptotic scaling regimes of interest, for freely evolving wave solutions or generated by a load moving on the ice (Dinvay, Kalisch & Părău 2019). Nonlinear dissipative models for wave attenuation in sea ice have also been investigated recently (Guyenne & Părău 2017; Alberello & Părău 2022; Alberello, Părău & Chabchoub 2023; Slunyaev & Stepanyants 2024).

We are interested here in the modulational regime where approximate solutions are sought in the form of slow modulations of near-monochromatic waves. In this case, perturbation calculations typically yield the nonlinear Schrödinger (NLS) equation which governs the nonlinear dispersive behaviour of the slowly varying wave envelope at leading order. The NLS equation is a canonical reduced model that arises in many areas of nonlinear science. Aside from its relative simplicity, its popularity owes much to its many mathematical properties, including a Hamiltonian formulation and exact travelling wave solutions such as envelope solitons.

Recent findings from both field observations and direct numerical simulations support the relevance of this modulational regime for wave–ice interactions in the ocean (Xu & Guyenne 2023). In particular, several sets of measurements from the Arctic Ocean have found that groupiness is a common trait of the wave field under open-water and ice-covered conditions (Gemmrich, Mudge & Thomson 2021). These observations even suggest that the group structure is enhanced when waves interact with sea ice. Wave groups with their inherent nonlinearity may be prone to wave focusing due to modulational instability and may produce unusually large amplitudes (Collins *et al.* 2015), which has implications for ice breaking and ice decline as well as for safety of ship navigation in the polar regions. Furthermore, this modulational approximation is of interest to the related problem where hydroelastic waves are induced by a moving load, having in mind, for example, frozen lakes that are used in winter for roads and aircraft runways. Experiments in Lake Saroma by Takizawa (1985) showed that a Ski-Doo snowmobile travelling at a certain speed generates localized disturbances of appreciable amplitude, which bear resemblance to solitary wave packets or envelope solitons.

For this hydroelastic problem, a body of work using modulation theory has developed NLS models in a variety of configurations. Pioneering results have been obtained by Liu & Mollo-Christensen (1988) and Marchenko & Shrira (1992), with the former authors considering nonlinear effects from ice bending, compression and inertia based on the Kirchhoff–Love (KL) formulation of a thin elastic plate, while the latter authors

incorporated linearized versions of these effects (without inertia). Nonlinear models based on KL theory have been widely used in both mathematical and numerical investigations. Subsequent examples include Părău & Dias (2002) who examined the response of a floating ice sheet to a moving load and derived a steady form of the NLS equation with a forcing term. They showed that solitary wave packets exist for certain ranges of parameter values. Milewski, Vanden-Broeck & Wang (2011) performed direct numerical simulations of the forced and unforced wave dynamics, with a focus on solutions having near-minimum phase speeds. They also produced asymptotic results based on a time-dependent NLS equation that was found to be of defocusing type at this minimum (i.e. for small-amplitude forcing) and was corroborated by the numerics. More recently, Slunyaev & Stepanyants (2022) proposed another NLS equation with a more elaborate elasticity model and identified in detail the domains of modulational instability for a broad range of physical parameters. Unlike Milewski *et al.* (2011) or Părău & Dias (2002), they adopted an extended version of the KL representation for ice bending and also included effects from ice compression and inertia. A similar parametric analysis was conducted by Hartmann *et al.* (2020) using the NLS equation of Liu & Mollo-Christensen (1988).

Alternatively, an important advance has been made by Plotnikov & Toland (2011) who devised a thin-plate formulation based on the special Cosserat theory of hyperelastic shells, coupled with nonlinear potential-flow theory for the fluid dynamics. A distinctive feature of their model as compared with KL is a more nonlinear dependence of the bending force exerted by the ice cover on the water surface, together with the fact that it has a conservative form. This allows such a model to be framed within the classical Hamiltonian formulation of the water wave problem by Zakharov (1968), providing a generalization to nonlinear hydroelastic waves. A number of subsequent studies have adopted Cosserat theory, including Guyenne & Părău (2012, 2014) and Milewski & Wang (2013) who conducted a weakly nonlinear analysis in the modulational regime and recovered earlier predictions from KL (Milewski *et al.* 2011) on the non-existence of small-amplitude wave packets (i.e. a defocusing NLS equation at the minimum phase speed).

Beyond the NLS equation in this asymptotic limit, the next-order approximation as originally proposed by Dysthe (1979) for surface gravity waves on deep water, has also drawn much attention and has since been extended to other settings. This so-called Dysthe equation has been shown to compare better with laboratory experiments and direct numerical simulations than the NLS equation does for larger wave steepnesses. For example, it can capture the asymmetry of evolving wave packets, whereas the NLS equation is unable to do so (Guyenne *et al.* 2021). Another effect arising at this higher level of approximation is the wave-induced mean flow which has an influence on the stability of finite-amplitude waves. However, unlike the NLS equation, earlier versions of the Dysthe equation lack a Hamiltonian structure that would comply with the primitive equations (i.e. the Euler system). Because it is desirable that important structural properties such as energy conservation be preserved for various reasons, recent effort has been devoted to establishing a Hamiltonian version of the Dysthe equation. In particular, Craig, Guyenne & Sulem (2021a), Guyenne, Kairzhan & Sulem (2022a) and Guyenne, Kairzhan & Sulem (2022b) developed a systematic approach to derive Hamiltonian Dysthe equations for water waves with or without a shear current by applying techniques from Hamiltonian perturbation theory, which involve reduction to normal form, homogenization and other canonical transformations. Such a reduction is achieved by eliminating non-resonant triads according to the linear dispersion relation. As a byproduct of this approach, the normal form transformation offers a non-perturbative procedure to reconstruct the surface elevation from the wave envelope, via the solution of an auxiliary Hamiltonian system of evolution equations. This contrasts with more standard techniques like the

method of multiple scales where the reconstruction is implemented perturbatively via a Stokes expansion. For hydroelastic waves, we are not aware of any previous report on a (Hamiltonian or non-Hamiltonian) Dysthe equation from the literature.

Pursuing this line of inquiry, the present work is an extension of Guyenne & Părău (2012) in several important directions. The starting point is a Hamiltonian formulation for nonlinear potential flow, coupled with a nonlinear representation of the ice cover based on Cosserat theory (Plotnikov & Toland 2011). Our viewpoint is motivated in part by the significance of Zakharov's Hamiltonian formulation which has formed the theoretical basis for a countless number of results on nonlinear water waves ranging from rigorous mathematical analysis to operational wave forecasting. The Dirichlet–Neumann operator (DNO) is introduced to accomplish the reduction to a lower-dimensional system in terms of surface variables, and its Taylor series expansion is exploited to carry out the perturbation calculations. We focus on the two-dimensional problem of hydroelastic waves on water of infinite depth. In this framework, our new contributions include the following.

- (i) Consideration of nonlinear models for both ice bending and compression, which is a refinement over previous studies based on simpler elasticity models (Marchenko & Shrira 1992; Milewski *et al.* 2011; Guyenne & Părău 2012; Milewski & Wang 2013). The competition between ice bending and compression can affect the focusing/defocusing nature of this modulational regime, with implications on the existence of solitary wave packets.
- (ii) Derivation of a Dysthe equation for the wave envelope, with a well-defined Hamiltonian structure and a conserved energy. This follows from a Birkhoff normal form transformation which is given by the explicit solution of a cohomological relation, involving an auxiliary system of integrodifferential equations in the Fourier space. An additional difficulty here is the presence of resonant cubic terms due to the more complicated dispersion relation.
- (iii) Development of a splitting scheme in the Fourier space to handle these resonant triads. Their detailed analysis leads to corrections in the normal form transformation as well as in the envelope equation, especially for the mean-flow term. Such corrections are absent in the pure gravity case (Craig *et al.* 2021a; Guyenne *et al.* 2022a) and differ fundamentally from previous adjustments to the Dysthe equation in similar situations such as gravity-capillary waves (Hogan 1985).
- (iv) Linear analysis of the modulational stability of Stokes waves in sea ice and validation against numerical solutions of the Dysthe equation under these conditions. A comparison with NLS predictions and with direct numerical simulations of the full Euler system is also presented. For this purpose, the surface reconstruction is accomplished in a non-perturbative manner by inverting the normal form transformation.

The remainder of this paper is organized as follows. The hydroelastic problem under consideration is described in § 2, including the Hamiltonian formulation in terms of the DNO, the Taylor expansion for small-amplitude waves and the linear dispersion relation. Section 3 examines the issue of cubic resonances and proposes a treatment in this theoretical setting. Section 4 presents the basic tools from Hamiltonian perturbation theory, focusing on the development of the Birkhoff normal form transformation to deal with resonant and non-resonant triads. The modulational ansatz for weakly nonlinear quasimonochromatic waves is introduced in § 5, and the Dysthe equation with its associated Hamiltonian is derived in § 6. Finally, § 7 gives an analytical prediction

on modulational instability, which is tested against numerical solutions of the Dysthe equation. This model's performance is also assessed relative to NLS computations and direct simulations of the full Euler system. Results are discussed for a range of ice and wave parameters.

2. Formulation of the problem

2.1. Equations of motion

We consider nonlinear hydroelastic waves propagating along an elastic sheet (e.g. ocean waves in sea ice) on top of a two-dimensional ideal fluid of infinite depth. In the thin-plate approximation, the ice sheet is assumed to coincide with the fluid surface $\{y = \eta(x, t)\}$ and to bend in unison with it. The fluid domain is then given by $S(\eta) := \{(x, y) : x \in \mathbb{R}, -\infty < y < \eta(x, t)\}$. Assuming that the fluid is incompressible, inviscid and irrotational, it is described by a potential flow such that the velocity field $\mathbf{u}(x, y, t) = \nabla\varphi$ satisfies

$$\nabla^2\varphi = 0, \quad (2.1)$$

in the fluid domain $S(\eta)$, where the symbol ∇ denotes the spatial gradient (∂_x, ∂_y) .

On the surface $y = \eta(x, t)$, we impose the standard kinematic condition

$$\partial_t\eta = \partial_y\varphi - (\partial_x\eta)(\partial_x\varphi), \quad (2.2)$$

as well as the dynamic boundary condition

$$\partial_t\varphi = -g\eta - \frac{1}{2} \left(\partial_x^2\varphi + \partial_y^2\varphi \right) - \mathcal{D} \left(\partial_s^2\kappa + \frac{1}{2}\kappa^3 \right) - \mathcal{P}\kappa. \quad (2.3)$$

This condition is derived from the Bernoulli balance of forces following Plotnikov & Toland (2011) for the interaction between an elastic ice sheet and water beneath it, while the compression term is proportional to the curvature of the fluid–ice interface. Here, g is the acceleration due to gravity, \mathcal{D} is the coefficient of flexural rigidity, \mathcal{P} is the coefficient of ice compression, κ is the curvature of the fluid–ice interface caused by the plate deflection and s is the arclength along this interface. The curvature κ , in terms of η , is given by

$$\kappa = \frac{\partial_x^2\eta}{(1 + (\partial_x\eta)^2)^{3/2}}, \quad (2.4)$$

so that the part in (2.3) that describes the bending of the ice sheet becomes

$$\begin{aligned} \partial_s^2\kappa + \frac{1}{2}\kappa^3 &= \frac{1}{\sqrt{1 + (\partial_x\eta)^2}} \partial_x \left(\frac{1}{\sqrt{1 + (\partial_x\eta)^2}} \partial_x \left(\frac{\partial_x^2\eta}{(1 + (\partial_x\eta)^2)^{3/2}} \right) \right) \\ &\quad + \frac{1}{2} \left(\frac{\partial_x^2\eta}{(1 + (\partial_x\eta)^2)^{3/2}} \right)^3. \end{aligned} \quad (2.5)$$

The boundary condition at the bottom reads

$$|\nabla\varphi| \rightarrow 0, \quad \text{as } y \rightarrow -\infty. \quad (2.6)$$

2.2. Hamiltonian formulation

Following Zakharov (1968) and Craig & Sulem (1993), the system of (2.2)–(2.6) has a Hamiltonian formulation in terms of the variables (η, ξ) , where $\xi(x, t) = \varphi(x, \eta(x, t), t)$ denotes the trace of the fluid velocity potential evaluated at the surface (Guyenne & Păruă 2012).

Indeed, introducing the DNO for the fluid domain, which associates with the Dirichlet data ξ on $y = \eta(x, t)$ the normal derivative of φ at the surface with a normalizing factor, namely

$$G(\eta) : \xi \mapsto \sqrt{1 + (\partial_x \eta)^2} \partial_n \varphi \Big|_{y=\eta}, \quad (2.7)$$

the equations of motion (2.2)–(2.3) are equivalent to the following canonical Hamiltonian system:

$$\partial_t \begin{pmatrix} \eta \\ \xi \end{pmatrix} = \begin{pmatrix} 0 & 1 \\ -1 & 0 \end{pmatrix} \begin{pmatrix} \partial_\eta H \\ \partial_\xi H \end{pmatrix}, \quad (2.8)$$

where the Hamiltonian $H(\eta, \xi)$ is the total energy

$$\begin{aligned} H(\eta, \xi) = & \frac{1}{2} \int_{\mathbb{R}} \xi G(\eta) \xi \, dx + \frac{1}{2} \int_{\mathbb{R}} \left(g\eta^2 + \mathcal{D} \frac{(\partial_x^2 \eta)^2}{(1 + (\partial_x \eta)^2)^{5/2}} \right. \\ & \left. - 2\mathcal{P} \left(\sqrt{1 + (\partial_x \eta)^2} - 1 \right) \right) \, dx. \end{aligned} \quad (2.9)$$

The first integral is the kinetic energy, while the second integral is the potential energy due to gravity, bending (or rigidity) and compression. The Hamiltonian H , together with the momentum

$$I = \int_{\mathbb{R}} \eta (\partial_x \xi) \, dx, \quad (2.10)$$

and the volume

$$V = \int_{\mathbb{R}} \eta \, dx, \quad (2.11)$$

are invariants of motion.

In Fourier variables, the system (2.8) preserves its canonical form. Indeed, denoting the Fourier transform of $f(x)$ by $\hat{f}_k = (1/\sqrt{2\pi}) \int_{\mathbb{R}} e^{-ikx} f(x) \, dx$, we have

$$\partial_t \begin{pmatrix} \hat{\eta}_{-k} \\ \hat{\xi}_{-k} \end{pmatrix} = \begin{pmatrix} 0 & 1 \\ -1 & 0 \end{pmatrix} \begin{pmatrix} \partial_{\hat{\eta}_k} H \\ \partial_{\hat{\xi}_k} H \end{pmatrix}, \quad (2.12)$$

where we have used that $(\hat{\eta}_{-k}, \hat{\xi}_{-k}) = (\bar{\hat{\eta}}_k, \bar{\hat{\xi}}_k)$ since $\eta(x)$ and $\xi(x)$ are real-valued functions. Due to the conservation of volume (2.11), we can choose $\hat{\eta}_0 = 0$. In the following, we drop the hats when denoting Fourier modes if there is no confusion.

2.3. Non-dimensionalization

The ice parameters are defined by

$$\mathcal{D} = \frac{\sigma}{\rho}, \quad \sigma = \frac{Eh^3}{12(1-\nu^2)}, \quad \mathcal{P} = \frac{Ph}{\rho}, \quad (2.13a-c)$$

where ρ is the density of the underlying fluid, h is the thickness of the ice sheet, ν is Poisson's ratio for ice, E is Young's modulus and P is the compressive stress. Numerical values of these physical parameters are listed in table 1 of Părău & Dias (2002) for two sets of experimental data. Introducing the characteristic length and time scales

$$\ell = \left(\frac{\sigma}{\rho g} \right)^{1/4} = \left(\frac{\mathcal{D}}{g} \right)^{1/4}, \quad \tau = \left(\frac{\sigma}{\rho g^5} \right)^{1/8} = \left(\frac{\mathcal{D}}{g^5} \right)^{1/8}, \quad (2.14a,b)$$

respectively (Guyenne & Părău 2012; Xu & Guyenne 2023), the dimensionless equations of motion follow (2.8) with Hamiltonian (2.9) modulo the change

$$\mathcal{P} \rightarrow \frac{Ph}{\sqrt{\sigma\rho g}} = \frac{\mathcal{P}}{\sqrt{g\mathcal{D}}}, \quad \mathcal{D} \rightarrow 1, \quad g \rightarrow 1, \quad (2.15)$$

where the first dimensionless parameter measures the relative importance of compression to gravity and rigidity. In typical physical situations, it is of order 1 (see for example Liu & Mollo-Christensen (1988) for realistic values of physical parameters and a discussion by Slunyaev & Stepanyants (2022)).

For convenience, we will use the same notations hereafter but it is understood that all variables and parameters are now dimensionless according to this choice of non-dimensionalization.

2.4. Taylor expansion of the Hamiltonian near equilibrium

It is known that the DNO is analytic in η (Coifman & Meyer 1985), and admits a convergent Taylor series expansion

$$G(\eta) = \sum_{m=0}^{\infty} G^{(m)}(\eta), \quad (2.16)$$

about $\eta = 0$. For each m , the term $G^{(m)}(\eta)$ is homogeneous of degree m in η , and can be calculated explicitly via recursive relations (Craig & Sulem 1993). Denoting $D = -i\partial_x$, the first three terms are

$$\left. \begin{aligned} G^{(0)}(\eta) &= |D|, \\ G^{(1)}(\eta) &= D\eta D - G^{(0)}\eta G^{(0)}, \\ G^{(2)}(\eta) &= -\frac{1}{2} \left(|D|^2 \eta^2 G^{(0)} + G^{(0)} \eta^2 |D|^2 - 2G^{(0)}\eta G^{(0)}\eta G^{(0)} \right). \end{aligned} \right\} \quad (2.17)$$

This in turn provides an expansion of the Hamiltonian near the stationary solution $(\eta, \xi) = (0, 0)$,

$$\begin{aligned} H(\eta, \xi) &= \frac{1}{2} \int_{\mathbb{R}} \left[\xi G^{(0)}(\eta) \xi + g\eta^2 + \mathcal{D}(\partial_x^2 \eta)^2 - \mathcal{P}(\partial_x \eta)^2 + \xi G^{(1)}(\eta) \xi \right. \\ &\quad \left. + \xi G^{(2)}(\eta) \xi - \frac{5}{2} \mathcal{D}(\partial_x \eta)^2 (\partial_x^2 \eta)^2 + \frac{1}{4} \mathcal{P}(\partial_x \eta)^4 + \dots \right] dx. \end{aligned} \quad (2.18)$$

In Fourier variables, the above expansion can be written as

$$H = H^{(2)} + H^{(3)} + H^{(4)} + \dots \quad (2.19)$$

where each term $H^{(m)}$ is homogeneous of degree m in η and ξ . In particular, we have

$$\left. \begin{aligned} H^{(2)} &= \frac{1}{2} \int \left(|k| |\xi_k|^2 + (g - \mathcal{P}k^2 + \mathcal{D}k^4) |\eta_k|^2 \right) dk, \\ H^{(3)} &= -\frac{1}{2\sqrt{2\pi}} \int (k_1 k_3 + |k_1| |k_3|) \xi_1 \eta_2 \xi_3 \delta_{123} dk_{123} \end{aligned} \right\} \quad (2.20)$$

and

$$\begin{aligned} H^{(4)} &= -\frac{1}{8\pi} \int |k_1| |k_4| (|k_1| + |k_4| - 2|k_3 + k_4|) \xi_1 \eta_2 \eta_3 \xi_4 \delta_{1234} dk_{1234} \\ &\quad + \frac{1}{4\pi} \int \left(\frac{5\mathcal{D}}{2} k_1^2 k_2^2 k_3 k_4 + \frac{\mathcal{P}}{4} k_1 k_2 k_3 k_4 \right) \eta_1 \eta_2 \eta_3 \eta_4 \delta_{1234} dk_{1234}, \end{aligned} \quad (2.21)$$

where we have used the compact notations $(\eta_j, \xi_j) = (\eta_{k_j}, \xi_{k_j})$, $dk_{1\dots n} = dk_1 \dots dk_n$ and $\delta_{1\dots n} = \delta(k_1 + \dots + k_n)$, where $\delta(\cdot)$ is the Dirac distribution $\delta(k) = (1/2\pi) \int_{\mathbb{R}} e^{-ikx} dx$. The domain of integration is now omitted from all integrals and is understood to be \mathbb{R} for each x_j or k_j . Notice that the ice parameters \mathcal{P} and \mathcal{D} appear explicitly in the expressions for $H^{(2)}$ and $H^{(4)}$, but not in $H^{(3)}$.

2.5. Dispersion relation

The linearized system for (2.8) around $(\eta, \xi) = (0, 0)$ is

$$\left. \begin{aligned} \partial_t \eta &= |D| \xi, \\ \partial_t \xi &= -g\eta - \mathcal{P} \partial_x^2 \eta - \mathcal{D} \partial_x^4 \eta. \end{aligned} \right\} \quad (2.22)$$

For

$$\omega^2(k) = \omega_k^2 := |k| \left(g - \mathcal{P}k^2 + \mathcal{D}k^4 \right), \quad (2.23)$$

equation (2.22) admits periodic plane-wave solutions

$$\eta(x, t) \propto e^{i(kx - \omega_k t)} \quad \text{and} \quad \xi(x, t) \propto e^{i(kx - \omega_k t)}. \quad (2.24a,b)$$

Equation (2.23) is known as the linear dispersion relation. By construction, for a particular choice of \mathcal{P} , \mathcal{D} and k the value of ω_k^2 may be either positive or negative. When ω_k^2 is positive, the solutions in (2.24a,b) are travelling waves since $\omega_k \in \mathbb{R}$. On the other hand, when $\omega_k^2 < 0$, one has $\omega_k \in i\mathbb{R}$, and therefore, the solutions in (2.24a,b) represent either evanescent or growing waves due to the factor $e^{\pm|\omega_k|t}$ in the expressions of η and ξ .

For parameters \mathcal{P} , \mathcal{D} and k with $\omega_k^2 > 0$, it is convenient to introduce the complex symplectic coordinates which diagonalize the quadratic Hamiltonian $H^{(2)}$ in (2.20).

In the Fourier space, these are given by

$$\begin{pmatrix} z_k \\ \bar{z}_{-k} \end{pmatrix} = \frac{1}{\sqrt{2}} \begin{pmatrix} a_k & i a_k^{-1} \\ a_k & -i a_k^{-1} \end{pmatrix} \begin{pmatrix} \eta_k \\ \xi_k \end{pmatrix}, \quad (2.25)$$

where $a_k^2 := \omega_k/|k|$. The quadratic term $H^{(2)}$ becomes

$$H^{(2)} = \int \omega_k |z_k|^2 dk, \quad (2.26)$$

while the cubic term $H^{(3)}$ takes the form

$$H^{(3)} = \frac{1}{8\sqrt{\pi}} \int (k_1 k_3 + |k_1||k_3|) \frac{a_1 a_3}{a_2} (z_1 - \bar{z}_{-1})(z_2 + \bar{z}_{-2})(z_3 - \bar{z}_{-3}) \delta_{123} dk_{123}, \quad (2.27)$$

where $z_{\pm j} := z_{\pm k_j}$ and $a_j := a_{k_j}$. Moreover, since the mapping (2.25) is canonical (Guyenne *et al.* 2022a), the full Hamiltonian system (2.12) becomes

$$\partial_t \begin{pmatrix} z_k \\ \bar{z}_{-k} \end{pmatrix} = \begin{pmatrix} 0 & -i \\ i & 0 \end{pmatrix} \begin{pmatrix} \partial_{z_k} H \\ \partial_{\bar{z}_{-k}} H \end{pmatrix}. \quad (2.28)$$

We note that the expressions (2.26) and (2.27) coincide in structure with the corresponding formulae for the quadratic and cubic Hamiltonians in the case of deep-water surface waves (Craig & Sulem 2016). This is because the parameters of ice rigidity and ice compression, appearing in our problem, are hidden in the definitions of ω_k and a_k .

One finds the values of \mathcal{P} when ω_k^2 is positive for any k by analysing the quartic inequality

$$\mathcal{D}k^4 - \mathcal{P}k^2 + g > 0. \quad (2.29)$$

Recall that $g = 1$ and $\mathcal{D} = 1$ in dimensionless units. For a given \mathcal{P} , one has $\omega_k^2 > 0$ for small or large k . When k takes moderate values, ω_k^2 could be negative. One can find the zeros of ω_k^2 analytically but it is more convenient to plot the dispersion relation ω_k^2 as a function of k for various values of the parameter \mathcal{P} as shown in figure 1. Note that ω_k^2 remains always positive whenever $\mathcal{P} < 2$. When $\mathcal{P} = 2$, $\omega_k^2 = 0$ for $k = 1$. A detailed analysis of the linear dispersion relation in terms of various physical parameters including ice bending and compression can also be found in Schulkes, Hosking & Sneyd (1987).

We are interested in having $\omega_k^2 > 0$ for all real values of k since we are looking for travelling wave solutions, not evanescent or growing waves. Thus, throughout the paper, we make the assumption

$$0 \leq \mathcal{P} < 2. \quad (2.30)$$

3. Resonant triads

3.1. Existence of resonant triads

We now address the question of existence of non-zero resonant triads (k_1, k_2, k_3) satisfying

$$k_1 + k_2 + k_3 = 0, \quad (3.1)$$

and at least one of the equations

$$\omega_1 \pm \omega_2 \pm \omega_3 = 0, \quad (3.2)$$

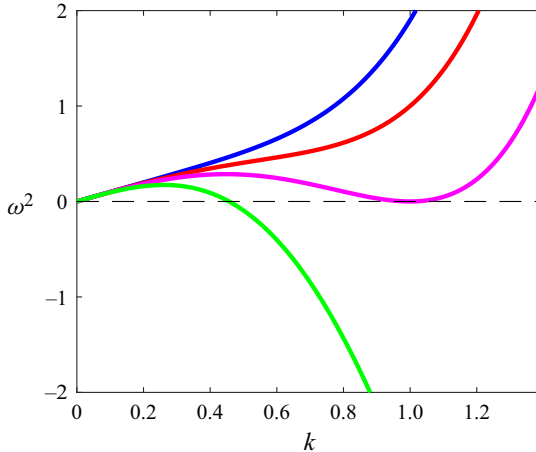


Figure 1. Linear dispersion relation $\omega^2(k)$ as a function of k for $\mathcal{P} = 0.1$ (blue), $\mathcal{P} = 1$ (red), $\mathcal{P} = 2$ (magenta), $\mathcal{P} = 5$ (green).

where ω_j stands for ω_{kj} . To find all the possible triads satisfying (3.1)–(3.2), we consider the following function:

$$d_{123} = d(k_1, k_2, k_3) := (\omega_1 + \omega_2 + \omega_3)(\omega_1 + \omega_2 - \omega_3)(\omega_1 - \omega_2 + \omega_3)(\omega_1 - \omega_2 - \omega_3). \quad (3.3)$$

From the construction of d_{123} , we have that (k_1, k_2, k_3) is a resonant triad if and only if it solves the system

$$\left. \begin{array}{l} k_1 + k_2 + k_3 = 0, \\ d(k_1, k_2, k_3) = 0, \\ k_j \neq 0, \quad j = \{1, 2, 3\}. \end{array} \right\} \quad (3.4)$$

The analogue of the system (3.4) was studied in detail by Craig & Sulem (2016) for surface gravity water waves. In that case, due to the absence of physical parameters \mathcal{P} and \mathcal{D} , the expression for d_{123} is much simpler and the computations can be performed by hand. However, in the present case, it is difficult to solve (3.4) explicitly due to the complexity of the dispersion relation (2.23) and the high degree of the polynomial function d_{123} .

Furthermore, as shown in Craig & Sulem (2016), the function d_{123} appears together with the constraint

$$k_1 k_3 + |k_1| |k_3| \neq 0. \quad (3.5)$$

Therefore, we provide estimates for d_{123} under the constraint (3.5) and the assumption $k_1 + k_2 + k_3 = 0$.

LEMMA 3.1. *Assuming $\text{sgn}(k_1) = \text{sgn}(k_3)$ and $k_1 + k_2 + k_3 = 0$, we have*

$$d_{123} = k_1 k_3 \tilde{d}(k_1, k_3), \quad (3.6)$$

where

$$\begin{aligned} \tilde{d}(k_1, k_3) := & k_1 k_3 (k_1 + k_3)^2 \left(3\mathcal{P} - 5\mathcal{D}(k_1^2 + k_1 k_3 + k_3^2) \right)^2 \\ & - 4(g - \mathcal{P}k_1^2 + \mathcal{D}k_3^4)(g - \mathcal{P}k_3^2 + \mathcal{D}k_1^4). \end{aligned} \quad (3.7)$$

The function \tilde{d} has the following symmetry properties:

$$\tilde{d}(k_1, k_3) = \tilde{d}(k_3, k_1) \quad \text{and} \quad \tilde{d}(k_1, k_3) = \tilde{d}(-k_1, -k_3). \quad (3.8a,b)$$

Proof. The results are based on direct computations under the above assumptions. Below, we provide a short overview of steps.

First, rewrite d_{123} as

$$d_{123} = (\omega_1^2 + \omega_3^2 - \omega_2^2)^2 - 4\omega_1^2\omega_3^2. \quad (3.9)$$

Observe that the second term on the right-hand side of (3.9) identifies with the second line in (3.7). For the first term on the right-hand side of (3.9), we write

$$\begin{aligned} \omega_1^2 + \omega_3^2 - \omega_2^2 &= g(|k_1| + |k_3| - |k_2|) - \mathcal{P}(|k_1|^3 + |k_3|^3 - |k_2|^3) \\ &\quad + \mathcal{D}(|k_1|^5 + |k_3|^5 - |k_2|^5). \end{aligned} \quad (3.10)$$

Given the assumptions, the first term vanishes since

$$|k_1| + |k_3| - |k_2| = 0, \quad (3.11)$$

and for the cubic terms, we have

$$|k_1|^3 + |k_3|^3 - |k_2|^3 = |k_2|(k_1^2 - k_1k_3 + k_3^2) - |k_2|^3 = -3|k_2|k_1k_3. \quad (3.12)$$

Similarly, for fifth-power terms, we have

$$|k_1|^5 + |k_3|^5 - |k_2|^5 = -5|k_2|k_1k_3(k_1^2 + k_1k_3 + k_3^2). \quad (3.13)$$

Substituting these expressions back into (3.9), we obtain (3.6). The properties (3.8a,b) are straightforward to verify.

Based on Lemma 3.1, finding resonant triads (k_1, k_2, k_3) in (3.4) under the constraint (3.5) is equivalent to finding the non-zero roots of the equation

$$\tilde{d}(k_1, k_3) = 0, \quad \text{with } \operatorname{sgn}(k_1) = \operatorname{sgn}(k_3), \quad (3.14)$$

where $k_2 = -k_1 - k_3$. Solving (3.14) explicitly seems to be impossible due to the complicated structure of $\tilde{d}(k_1, k_3)$ in (3.7). Therefore, we find solutions to (3.14) numerically. Since \tilde{d} is invariant under sign change of variables, $\tilde{d}(k_1, k_3) = \tilde{d}(-k_1, -k_3)$, we only concentrate on the positive roots of (3.14) and the negative roots are found by symmetry. Setting $\mathcal{P} = 1$ for simplicity, the solution curve \mathcal{C}^+ for positive roots of (3.14) is displayed in figure 2. A similar solution curve is present for other values of $\mathcal{P} < 2$. We note that the curve \mathcal{C}^+ is unbounded, has the k_1 - and k_3 -axes as asymptotes and never intersects these axes. The negative roots of (3.14) are given by the solution curve \mathcal{C}^- , which is obtained from \mathcal{C}^+ by symmetry with respect to the origin. Combining these curves, all non-zero roots of (3.14) are given by

$$\mathcal{C} := \mathcal{C}^+ \cup \mathcal{C}^-. \quad (3.15)$$

In our analysis later, various integrals involve expressions where the function $\tilde{d}(k_1, k_3)$ appears in the denominator. To avoid this ‘small divisors’ issue, we will restrict the integral

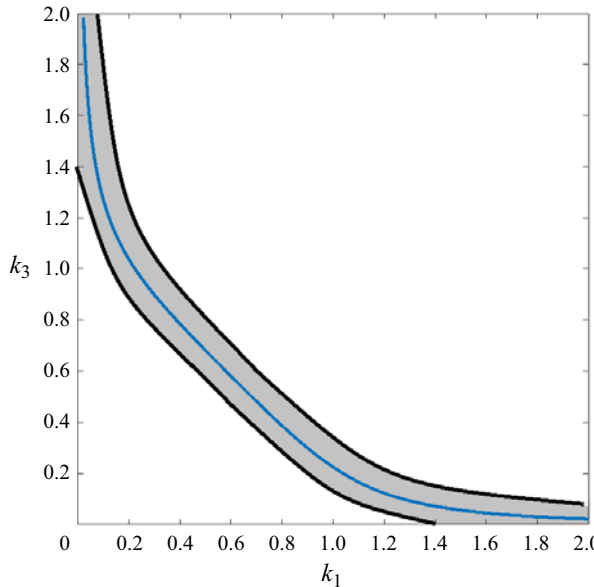


Figure 2. Solution curve \mathcal{C}^+ (blue curve) for positive roots (k_1, k_3) of (3.14) and its neighbourhood \mathcal{C}_μ^+ (grey area) for $\mathcal{P} = 1$.

to regions away from the solution curve \mathcal{C} . To do so, we construct a neighbourhood of \mathcal{C} , referred to as \mathcal{C}_μ , for sufficiently small μ , such that

$$|\tilde{d}(x, y)| \geq \text{const.}_\mu, \quad \text{for all } (x, y) \in \mathbb{R}^2 \setminus \mathcal{C}_\mu, \quad (3.16)$$

where const._μ is a constant depending on μ only. More precisely, at every point $(k_1, k_3) \in \mathcal{C}^+$, denote a normal vector to \mathcal{C}^+ by $\mathbf{n}(k_1, k_3)$. Then, consider the set of points in the (k_1, k_3) -plane given by

$$\{(k_1, k_3) + \mu t \mathbf{n}(k_1, k_3) : t \in [-1, 1] \text{ and } (k_1, k_3) \in \mathcal{C}^+\}, \quad (3.17)$$

which geometrically looks like a ‘tube’ around the curve \mathcal{C}^+ with a width μ . We then construct a neighbourhood of \mathcal{C}^+ , denoted by \mathcal{C}_μ^+ , as

$$\mathcal{C}_\mu^+ := \{\text{the set (3.17)}\} \cap \{(x, y) : x \geq 0, y \geq 0\}. \quad (3.18)$$

A sketch of \mathcal{C}_μ^+ is shown in figure 2 for $\mathcal{P} = 1$. The neighbourhood \mathcal{C}_μ^- for the curve \mathcal{C}^- is constructed similarly, and can be seen as the reflection of \mathcal{C}_μ^+ with respect to the origin. Combining these sets, we get the neighbourhood of the set \mathcal{C} in (3.15) as $\mathcal{C}_\mu := \mathcal{C}_\mu^+ \cup \mathcal{C}_\mu^-$.

We now provide formal arguments to show that (3.16) is satisfied for the set \mathcal{C}_μ constructed above. It suffices to show that (3.16) is satisfied on the boundary of \mathcal{C}_μ for small values of k_1 , which corresponds to the far end of the neighbourhood in figure 2 located at the top left-hand corner. Then, the validity of (3.16) for all (x, y) outside \mathcal{C}_μ follows by continuity arguments and symmetry.

First, we note that, under assumption (2.30), the points $(k_1, k_3) \in \mathcal{C}$ satisfy $k_3 \approx (4g/(25Dk_1))^{1/3}$ whenever $k_1 \ll 1$. Indeed, from (3.7), it is clear that if $k_1 \ll 1$ then

$k_3 \gg 1$. As a result, for $k_1 \ll 1$, we have

$$0 = \tilde{d}(k_1, k_3) \approx 25\mathcal{D}^2 k_1 k_3^7 - 4g\mathcal{D} k_3^4 \implies k_3 \approx \left(\frac{4g}{25\mathcal{D} k_1} \right)^{1/3}. \quad (3.19)$$

Therefore, the normal vector of \mathcal{C}^+ for small values of k_1 is approximately given by

$$\mathbf{n}(k_1, k_3) = \frac{\left(k_1, 3k_1^{4/3} \left(\frac{25\mathcal{D}}{4g} \right)^{1/3} \right)}{\left\| k_1, 3k_1^{4/3} \left(\frac{25\mathcal{D}}{4g} \right)^{1/3} \right\|} \approx (1, 0). \quad (3.20)$$

The points on the boundary of \mathcal{C}_μ^+ with $k_1 \ll 1$ are

$$(0, k_3) \quad \text{and} \quad (k_1 + \mu, k_3), \quad (3.21)$$

where k_3 satisfies the estimate (3.19). Applying simple algebraic steps to (3.7), it can be shown that the value of $\tilde{d}(0, k_3)$ under the assumption (2.30) is bounded away from zero by

$$\left| \tilde{d}(0, k_3) \right| \geq \left| \tilde{d}(0, \sqrt{\mathcal{P}/(2\mathcal{D})}) \right| = \frac{g}{\mathcal{D}} (4g\mathcal{D} - \mathcal{P}^2) > 0. \quad (3.22)$$

To estimate the value of $\tilde{d}(k_1 + \mu, k_3)$ we use the Taylor expansion

$$\tilde{d}(k_1 + \mu, k_3) \approx \tilde{d}(k_1, k_3) + \mu \partial_{k_1} \tilde{d}(k_1, k_3) = \mu \partial_{k_1} \tilde{d}(k_1, k_3). \quad (3.23)$$

Taking the derivative of (3.7) with respect to k_1 , we have

$$\begin{aligned} \partial_{k_1} \tilde{d}(k_1, k_3) &= k_3 (3k_1 + k_3) (k_1 + k_3) \left(3\mathcal{P} - 5\mathcal{D}(k_1^2 + k_1 k_3 + k_3^2) \right)^2 \\ &\quad - 10k_1 k_3 (k_1 + k_3)^2 \left(3\mathcal{P} - 5\mathcal{D}(k_1^2 + k_1 k_3 + k_3^2) \right) \mathcal{D} (2k_1 + k_3) \\ &\quad + 4(2\mathcal{P}k_1 - 4\mathcal{D}k_1^3)(g - \mathcal{P}k_3^2 + \mathcal{D}k_3^4), \end{aligned} \quad (3.24)$$

which, under (3.19), is approximated by

$$\partial_{k_1} \tilde{d}(k_1, k_3) \approx 25\mathcal{D}^2 k_3^7, \quad (3.25)$$

whenever $k_1 \ll 1$. As a result, the estimate in (3.23) takes the form

$$\tilde{d}(k_1 + \mu, k_3) \approx 25\mu\mathcal{D}^2 k_3^7, \quad (3.26)$$

which is bounded away from zero as desired. Later in the analysis, the function d_{123} will appear in the denominator and we will set $\mu = \varepsilon$, where ε is the small parameter in the modulational regime.

In view of (3.4) and (3.6), the set of resonant triads satisfying (3.1)–(3.2) is given by

$$\mathcal{R} := \{(k_1, -k_1 - k_3, k_3) \in \mathbb{R}^3 : (k_1, k_3) \in \mathcal{C}\}. \quad (3.27)$$

The neighbourhood of \mathcal{R} is defined by

$$\mathcal{N}_\mu := \{(k_1, -k_1 - k_3, k_3) \in \mathbb{R}^3 : (k_1, k_3) \in \mathcal{C}_\mu\}, \quad (3.28)$$

as illustrated in figure 2. We also define a characteristic function $\chi_{\mathcal{N}_\mu}(k_1, k_2, k_3)$ supported in the neighbourhood \mathcal{N}_μ as

$$\chi_{\mathcal{N}_\mu}(k_1, k_2, k_3) := \begin{cases} 1, & \text{if } (k_1, k_2, k_3) \in \mathcal{N}_\mu, \\ 0, & \text{otherwise.} \end{cases} \quad (3.29)$$

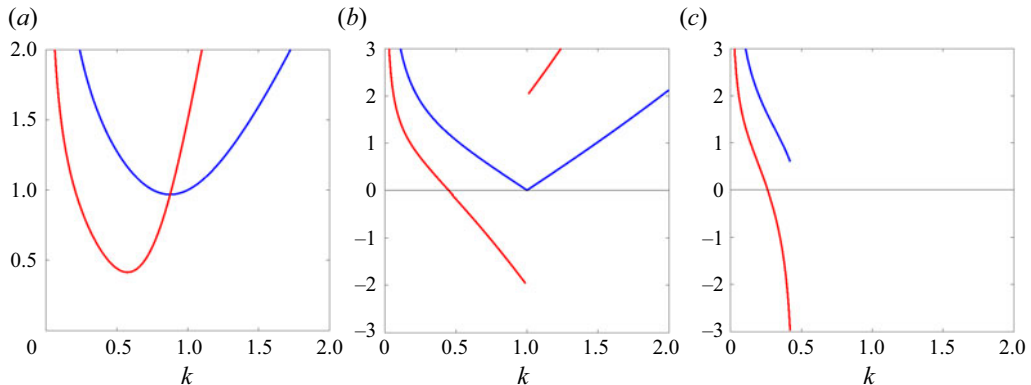


Figure 3. Phase speed $c(k)$ (blue) and group speed $c_g(k)$ (red) as functions of k for (a) $\mathcal{P} = 1$, (b) $\mathcal{P} = 2$, (c) $\mathcal{P} = 5$.

3.2. Phase and group speeds

Assuming $k > 0$ without loss of generality (since ω_k is an even function of k), the phase speed associated with the linear dispersion relation (2.23) is given by

$$c(k) = \frac{\omega_k}{k} = \sqrt{\frac{g - \mathcal{P}k^2 + \mathcal{D}k^4}{k}}, \quad (3.30)$$

while the group speed reads

$$c_g(k) = \partial_k \omega_k = \frac{g - 3\mathcal{P}k^2 + 5\mathcal{D}k^4}{2\omega_k}. \quad (3.31)$$

It can be easily shown that, if the phase speed c has a local minimum at $k = k_{min}$, then the phase and group speeds coincide at this minimum. The equation $c = c_g$ reduces to $g + \mathcal{P}k^2 - 3\mathcal{D}k^4 = 0$ which is quadratic in k^2 . The only possible solution that is real and positive takes the form

$$k_{min} = \sqrt{\frac{\mathcal{P} + \sqrt{\mathcal{P}^2 + 12g\mathcal{D}}}{6\mathcal{D}}}. \quad (3.32)$$

In the flexural-gravity case ($\mathcal{P} = 0$), this solution yields the well-known value $k_{min} = (g/(3\mathcal{D}))^{1/4}$ (Guyenne & Părău 2012). Figure 3 shows the phase and group speeds for values $\mathcal{P} = \{1, 2, 5\}$.

4. Transformation theory

The method of Hamiltonian transformation theory has been previously applied to deep-water irrotational gravity waves in two and three dimensions (Craig *et al.* 2021a; Guyenne *et al.* 2022a), and waves with constant vorticity (Guyenne *et al.* 2022b) to derive a Hamiltonian Dysthe equation for the envelope of the surface elevation. In all of these cases, the set of resonant triads, satisfying the analogue of (3.2), is either empty or naturally ruled out from the analysis. This is not the case in the present problem.

We recall that the Poisson bracket of two functionals $K(\eta, \xi)$ and $H(\eta, \xi)$ of real-valued functions η and ξ is defined as

$$\{K, H\} = \int (\partial_\eta H \partial_\xi K - \partial_\xi H \partial_\eta K) \, dx. \quad (4.1)$$

Assuming in addition that K and H are real-valued, the Poisson bracket takes the form

$$\begin{aligned} \{K, H\} &= \int (\partial_{\eta_{k_1}} H \partial_{\xi_{k_2}} K - \partial_{\xi_{k_1}} H \partial_{\eta_{k_2}} K) \delta_{12} \, dk_{12}, \\ &= \frac{1}{i} \int (\partial_{z_{k_1}} H \partial_{\bar{z}_{-k_2}} K - \partial_{\bar{z}_{-k_1}} H \partial_{z_{k_2}} K) \delta_{12} \, dk_{12}. \end{aligned} \quad (4.2)$$

4.1. Canonical transformation

We first construct a transformation that eliminates non-resonant terms from the cubic Hamiltonian (2.27). More precisely, we are looking for a canonical transformation of the physical variables (η, ξ)

$$\tau : w = \begin{pmatrix} \eta \\ \xi \end{pmatrix} \longmapsto w' = \begin{pmatrix} \eta' \\ \xi' \end{pmatrix}, \quad (4.3)$$

defined in a neighbourhood of the origin, such that the transformed Hamiltonian satisfies

$$H'(w') = H(\tau^{-1}(w')), \quad \partial_t w' = J \nabla H'(w'), \quad (4.4a,b)$$

and reduces to

$$H'(w') = H^{(2)}(w') + Z^{(3)} + Z^{(4)} + \cdots + Z^{(m)} + R^{(m+1)}, \quad (4.5)$$

where $Z^{(j)}$ only consists of resonant terms of order j and $R^{(m+1)}$ is the remainder term at order m (Craig & Sulem 2016; Craig, Guyenne & Sulem 2021b). The transformation τ is obtained as a Hamiltonian flow ψ from ‘time’ $s = -1$ to ‘time’ $s = 0$ governed by

$$\partial_s \psi = J \nabla K(\psi), \quad \psi(w')|_{s=0} = w', \quad \psi(w')|_{s=-1} = w, \quad (4.6)$$

and associated with an auxiliary Hamiltonian K . Such a transformation is canonical and preserves the Hamiltonian structure of the system. The Hamiltonian H' satisfies $H'(w') = H(\psi(w'))|_{s=-1}$ and its Taylor expansion around $s = 0$ is

$$H'(w') = H(\psi(w'))|_{s=0} - \frac{dH}{ds}(\psi(w'))|_{s=0} + \frac{1}{2} \frac{d^2H}{ds^2}(\psi(w'))|_{s=0} - \cdots. \quad (4.7)$$

Abusing notations, we further drop the primes and use $w = (\eta, \xi)^\top$ to denote the new variable w' . Terms in this expansion can be expressed using Poisson brackets as

$$\begin{aligned} H(\psi(w))|_{s=0} &= H(w), \\ \frac{dH}{ds}(\psi(w))|_{s=0} &= \int (\partial_\eta H \partial_s \eta + \partial_\xi H \partial_s \xi) \, dx, \\ &= \int (\partial_\eta H \partial_\xi K - \partial_\xi H \partial_\eta K) \, dx = \{K, H\}(w), \end{aligned} \quad (4.8)$$

and similar expressions can be obtained for higher-order s -derivatives. The Taylor expansion of H' around $s = 0$ now has the form

$$H'(w) = H(w) - \{K, H\}(w) + \frac{1}{2}\{K, \{K, H\}\}(w) - \dots \quad (4.9)$$

Substituting this transformation into the expansion (2.19) of H , we obtain

$$\begin{aligned} H'(w) &= H^{(2)}(w) + H^{(3)}(w) + \dots \\ &\quad - \{K, H^{(2)}\}(w) - \{K, H^{(3)}\}(w) - \{K, H^{(4)}\}(w) - \dots \\ &\quad + \frac{1}{2}\{K, \{K, H^{(2)}\}\}(w) + \frac{1}{2}\{K, \{K, H^{(3)}\}\}(w) + \dots \end{aligned} \quad (4.10)$$

If K is homogeneous of degree m and $H^{(n)}$ is homogeneous of degree n , then $\{K, H^{(n)}\}$ is of degree $m + n - 2$. Thus, if we construct an auxiliary Hamiltonian $K = K^{(3)}$ that is homogeneous of degree 3 and satisfies the relation

$$H^{(3)} - \{K^{(3)}, H^{(2)}\} = 0, \quad (4.11)$$

we will have eliminated all cubic terms from the transformed Hamiltonian H' . We can repeat this process at each order.

4.2. Third-order Birkhoff normal form

We recall that the complex symplectic coordinates z_j and \bar{z}_{-j} diagonalize the coadjoint operator $\text{coad}_{H^{(2)}} := \{\cdot, H^{(2)}\}$, that is, the linear operation of taking Poisson brackets with $H^{(2)}$ (Craig & Sulem 2016; Guyenne *et al.* 2022a). When applying the operator to monomial terms such as $\mathcal{I} := \int z_1 z_2 \bar{z}_{-3} \delta_{123} dk_{123}$, we have

$$\{\mathcal{I}, H^{(2)}\} = i \int (\omega_1 + \omega_2 - \omega_3) z_1 z_2 \bar{z}_{-3} \delta_{123} dk_{123}. \quad (4.12)$$

We use the diagonal property as in (4.12) to find the auxiliary Hamiltonian $K^{(3)}$ from (4.11). The presence of resonant triads (3.27) does not allow us to eliminate $H^{(3)}$ completely by virtue of (4.11). Instead, we are only able to find $K^{(3)}$ such that

$$\{K^{(3)}, H^{(2)}\} = H_{NoRes}^{(3)}, \quad (4.13)$$

where $H_{NoRes}^{(3)}$ stands for the non-resonant part of the third-order Hamiltonian. Explicitly, we define the non-resonant part of $H^{(3)}$ as $H_{NoRes}^{(3)} := H^{(3)} - H_{Res}^{(3)}$, where

$$H_{Res}^{(3)} = \frac{1}{8\sqrt{\pi}} \int \chi_{\mathcal{N}_\mu}(k_1, k_2, k_3) S_{123} (z_1 \bar{z}_{-2} z_3 + \bar{z}_{-1} z_2 \bar{z}_{-3}) \delta_{123} dk_{123}, \quad (4.14)$$

is a resonant part of (2.27),

$$S_{123} = S(k_1, k_2, k_3) := (k_1 k_3 + |k_1||k_3|) \frac{a_1 a_3}{a_2}, \quad (4.15)$$

and $\chi_{\mathcal{N}_\mu}$ is the characteristic function defined in (3.29).

PROPOSITION 4.1. *The cohomological equation (4.13) has a unique solution $K^{(3)}$ which, in complex symplectic coordinates, is*

$$K^{(3)} = \frac{1}{8i\sqrt{\pi}} \int S_{123} \left[\frac{z_1 z_2 z_3 - \bar{z}_{-1} \bar{z}_{-2} \bar{z}_{-3}}{\omega_1 + \omega_2 + \omega_3} - 2 \frac{z_1 z_2 \bar{z}_{-3} - \bar{z}_{-1} \bar{z}_{-2} z_3}{\omega_1 + \omega_2 - \omega_3} + (1 - \chi_{\mathcal{N}_\mu}(k_1, k_2, k_3)) \frac{z_1 \bar{z}_{-2} z_3 - \bar{z}_{-1} z_2 \bar{z}_{-3}}{\omega_1 - \omega_2 + \omega_3} \right] \delta_{123} dk_{123}. \quad (4.16)$$

Alternatively, in the variables (η, ξ) , $K^{(3)}$ has the form

$$K^{(3)} = \frac{1}{\sqrt{2\pi}} \int (P_{123} \eta_1 \eta_2 \xi_3 + Q_{123} \eta_1 \xi_2 \eta_3 + R_{123} \xi_1 \xi_2 \xi_3) \delta_{123} dk_{123}, \quad (4.17)$$

where the denominator d_{123} is given in (3.3) and the coefficients are

$$\left. \begin{aligned} P_{123} &= \frac{1 + \text{sgn}(k_1)\text{sgn}(k_3)}{4\tilde{d}(k_1, k_3)} a_1^2 \left(4\omega_1(\omega_1^2 - \omega_2^2 - \omega_3^2) - \chi_{\mathcal{N}_\mu}(k_1, k_2, k_3) \Pi_{123} \right), \\ Q_{123} &= \frac{1 + \text{sgn}(k_1)\text{sgn}(k_3)}{8\tilde{d}(k_1, k_3)} \left(\frac{a_1^2 a_3^2}{a_2^2} \right) \left(8\omega_1\omega_2\omega_3 + \chi_{\mathcal{N}_\mu}(k_1, k_2, k_3) \Pi_{123} \right), \\ R_{123} &= \frac{1 + \text{sgn}(k_1)\text{sgn}(k_3)}{8\tilde{d}(k_1, k_3)} \left(\frac{1}{a_2^2} \right) \left(4\omega_2(\omega_1^2 - \omega_2^2 + \omega_3^2) - \chi_{\mathcal{N}_\mu}(k_1, k_2, k_3) \Pi_{123} \right), \end{aligned} \right\} \quad (4.18)$$

with $\Pi_{123} := (\omega_1 + \omega_2 + \omega_3)(\omega_1 + \omega_2 - \omega_3)(\omega_1 - \omega_2 - \omega_3)$.

Proof. The derivations of (4.16) and (4.17) are based on straightforward computations. The expression (4.16) is obtained by applying the diagonal property (4.12) to the non-resonant part of the cubic Hamiltonian, $H_{NoRes}^{(3)}$. The expression (4.17) is derived from (4.16) by substituting the relation (2.25).

We point out that the coefficients P_{123} , Q_{123} and R_{123} are well defined in the neighbourhood of the resonant triads (3.27). This is due to the construction of $K^{(3)}$ in (4.16) which avoids the resonant triads that make the denominator $\omega_1 - \omega_2 + \omega_3$ equal to 0. This is the principal reason why we solve (4.13) to find $K^{(3)}$ rather than the full relation $\{K^{(3)}, H^{(2)}\} = H^{(3)}$ in (4.11). The latter equation would lead to an ill-defined $K^{(3)}$ with vanishing denominator $\omega_1 - \omega_2 + \omega_3$, which we cannot handle.

The third-order normal form defining the new coordinates is obtained as the solution map at $s = 0$ of the Hamiltonian flow

$$\partial_s \begin{pmatrix} \eta \\ \xi \end{pmatrix} = \begin{pmatrix} 0 & 1 \\ -1 & 0 \end{pmatrix} \begin{pmatrix} \partial_\eta K^{(3)} \\ \partial_\xi K^{(3)} \end{pmatrix}, \quad (4.19)$$

with initial condition at $s = -1$ being the original variables (η, ξ) . Equivalently, in Fourier coordinates,

$$\partial_s \eta_{-k} = \partial_{\xi_k} K^{(3)}, \quad \partial_s \xi_{-k} = -\partial_{\eta_k} K^{(3)}, \quad (4.20a,b)$$

where

$$\left. \begin{aligned} \partial_{\xi_k} K^{(3)} &= \frac{1}{\sqrt{2\pi}} \int ((P_{12k} + Q_{1k2}) \eta_1 \eta_2 + (R_{12k} + R_{2k1} + R_{k12}) \xi_1 \xi_2) \delta_{12k} dk_{12}, \\ \partial_{\eta_k} K^{(3)} &= \frac{1}{\sqrt{2\pi}} \int (P_{1k2} + P_{k12} + Q_{12k} + Q_{k21}) \eta_1 \xi_2 \delta_{12k} dk_{12}, \end{aligned} \right\} \quad (4.21)$$

by virtue of (4.17).

5. Reduced Hamiltonian

The new Hamiltonian H' obtained after applying the third-order normal form transformation has the form

$$\begin{aligned} H(w) &= H^{(2)}(w) + H_{Res}^{(3)}(w) + H^{(4)}(w) - \{K^{(3)}, H^{(3)}\}(w) \\ &\quad + \frac{1}{2} \{K^{(3)}, \{K^{(3)}, H^{(2)}\}\}(w) + R^{(5)} \\ &= H^{(2)}(w) + H_{Res}^{(3)}(w) + H_+^{(4)}(w) + R^{(5)}, \end{aligned} \quad (5.1)$$

where $R^{(5)}$ denotes all terms of order 5 and higher, and $H_+^{(4)}$ is the new fourth-order term

$$H_+^{(4)} = H^{(4)} - \frac{1}{2} \{K^{(3)}, H_{NoRes}^{(3)}\} - \{K^{(3)}, H_{Res}^{(3)}\}, \quad (5.2)$$

where we have used the relation (4.13). Note that the presence of resonant terms did not eliminate all homogeneous cubic terms in H , and the resonant terms also contribute to the quartic part of the Hamiltonian.

In view of the forthcoming modulational ansatz, the only important quartic terms are given by

$$H_{+R}^{(4)} = \int T z_1 z_2 \bar{z}_3 \bar{z}_4 \delta_{1+2-3-4} dk_{1234}. \quad (5.3)$$

The other quartic terms will not contribute under this ansatz due to homogenization; we refer to § 4 of Guyenne *et al.* (2022a) for details. In § 5.3, we show that the resonant cubic Hamiltonian $H_{Res}^{(3)}$ in (5.1) can also be ruled out of the computations. As a result, the Hamiltonian H in (5.1) is at leading order

$$H(w) = H^{(2)}(w) + H_{+R}^{(4)}(w) + \tilde{R}. \quad (5.4)$$

Denoting

$$H_R^{(4)} = \int T_0 z_1 z_2 \bar{z}_3 \bar{z}_4 \delta_{1+2-3-4} dk_{1234}, \quad (5.5)$$

$$\left. \begin{aligned} \{K^{(3)}, H_{NoRes}^{(3)}\}_R &= \int T_{NoRes} z_1 z_2 \bar{z}_3 \bar{z}_4 \delta_{1+2-3-4} dk_{1234}, \\ \{K^{(3)}, H_{Res}^{(3)}\}_R &= \int T_{Res} z_1 z_2 \bar{z}_3 \bar{z}_4 \delta_{1+2-3-4} dk_{1234}, \end{aligned} \right\} \quad (5.6)$$

the contributions of $z z z \bar{z} \bar{z}$ -type monomials to the terms of (5.2), we have that T appearing in (5.3) identifies to

$$T = T_0 - \frac{1}{2} T_{NoRes} - T_{Res}. \quad (5.7)$$

5.1. Explicit computations of T_0 , T_{Res} and T_{NoRes}

Here, we provide precise formulae for the coefficients T_0 , T_{Res} and T_{NoRes} appearing in (5.5)–(5.6).

PROPOSITION 5.1. *We have $T_0 = T_0^{(1)} + T_0^{(2)}$, where*

$$\left. \begin{aligned} T_0^{(1)} &= -V_{12(-3)(-4)} - V_{(-4)(-3)21} - V_{1(-3)2(-4)} - V_{(-4)2(-3)1} \\ &\quad + V_{1(-4)(-3)2} + V_{(-3)21(-4)}, \\ T_0^{(2)} &= \frac{k_1 k_2 k_3 k_4}{32\pi a_1 a_2 a_3 a_4} (5\mathcal{D}(k_1 k_2 - k_1 k_3 - k_1 k_4 - k_2 k_3 - k_2 k_4 + k_3 k_4) - 3\mathcal{P}), \end{aligned} \right\} \quad (5.8)$$

with

$$V_{1234} = \frac{a_1 a_4}{32\pi a_2 a_3} |k_1| |k_4| (|k_1| + |k_4| - 2|k_3 + k_4|). \quad (5.9)$$

Proof. The proof is given in [Appendix B](#).

PROPOSITION 5.2. *Let $B_{123} := S_{123}(1 - \chi_{\mathcal{N}_\mu}(k_1, k_2, k_3))$ with S_{123} and $\chi_{\mathcal{N}_\mu}$ given in (4.15) and (3.29), respectively. Then, $T_{NoRes} = T_{NoRes}^{(1)} + T_{NoRes}^{(2)} + T_{NoRes}^{(3)}$ with*

$$\begin{aligned} T_{NoRes}^{(1)} &= \frac{1}{64\pi} (S_{(-1-2)12} + S_{2(-1-2)1} + S_{12(-1-2)}) (S_{(-3-4)34} + S_{4(-3-4)3} + S_{34(-3-4)}) \\ &\quad \times \left(\frac{1}{\omega_1 + \omega_2 + \omega_{1+2}} + \frac{1}{\omega_3 + \omega_4 + \omega_{3+4}} \right) \\ &\quad + \frac{1}{16\pi} (S_{(3-1)(-3)1} + S_{1(3-1)(-3)}) (S_{(4-2)2(-4)} + S_{(-4)(4-2)2}) \\ &\quad \times \left(\frac{1}{\omega_{3-1} + \omega_3 - \omega_1} + \frac{1}{\omega_{4-2} + \omega_2 - \omega_4} \right) \\ &\quad - \frac{1}{16\pi} S_{12(-1-2)} S_{34(-3-4)} \left(\frac{1}{\omega_1 + \omega_2 - \omega_{1+2}} + \frac{1}{\omega_3 + \omega_4 - \omega_{3+4}} \right), \end{aligned} \quad (5.10)$$

$$\begin{aligned} T_{NoRes}^{(2)} &= \frac{1}{32\pi} (S_{12(-1-2)} B_{3(-3-4)4} + S_{34(-3-4)} B_{1(-1-2)2}) \\ &\quad \times \left(\frac{1}{\omega_1 + \omega_2 - \omega_{1+2}} + \frac{1}{\omega_3 + \omega_4 - \omega_{3+4}} \right) \\ &\quad - \frac{1}{16\pi} B_{(4-2)(-4)2} (S_{(3-1)(-3)1} + S_{(-3)(3-1)1}) \\ &\quad \times \left(\frac{1}{\omega_{3-1} + \omega_3 - \omega_1} + \frac{1}{\omega_{4-2} + \omega_2 - \omega_4} \right) \\ &\quad - \frac{1}{16\pi} B_{(3-1)1(-3)} (S_{(4-2)2(-4)} + S_{2(4-2)(-4)}) \\ &\quad \times \left(\frac{1}{\omega_{3-1} + \omega_3 - \omega_1} + \frac{1}{\omega_{4-2} + \omega_2 - \omega_4} \right) \end{aligned} \quad (5.11)$$

and

$$\begin{aligned} T_{NoRes}^{(3)} = & -\frac{1}{64\pi} B_{1(-1-2)2} B_{3(-3-4)4} \left(\frac{1}{\omega_1 + \omega_2 - \omega_{1+2}} + \frac{1}{\omega_3 + \omega_4 - \omega_{3+4}} \right) \\ & + \frac{1}{16\pi} B_{(3-1)1(-3)} B_{(4-2)(-4)2} \left(\frac{1}{\omega_{3-1} + \omega_3 - \omega_1} + \frac{1}{\omega_{4-2} + \omega_2 - \omega_4} \right). \end{aligned} \quad (5.12)$$

Here, based on (4.15), $S_{(3-1)(-3)1}$ reads

$$S_{(3-1)(-3)1} = ((k_3 - k_1)k_1 + |k_3 - k_1||k_1|) \frac{a(k_3 - k_1)a(k_1)}{a(-k_3)}, \quad (5.13)$$

and $B_{(3-1)(-3)1} = S_{(3-1)(-3)1}(1 - \chi_{\mathcal{N}_\mu}(k_3 - k_1, -k_3, k_1))$.

Proof. The proof is given in [Appendix C](#).

PROPOSITION 5.3. Recall that S_{123} is given by (4.15) and $B_{123} := S_{123}(1 - \chi_{\mathcal{N}_\mu}(k_1, k_2, k_3))$. Then, $T_{Res} = T_{Res}^{(1)} + T_{Res}^{(2)}$ with

$$\begin{aligned} T_{Res}^{(1)} = & \frac{1}{32\pi} \left(\frac{S_{12(-1-2)}}{\omega_1 + \omega_2 - \omega_{1+2}} [\chi S]_{3(-3-4)4} + \frac{S_{34(-3-4)}}{\omega_3 + \omega_4 - \omega_{3+4}} [\chi S]_{1(-1-2)2} \right) \\ & - \frac{1}{16\pi(\omega_{3-1} + \omega_3 - \omega_1)} (S_{(3-1)(-3)1} + S_{(-3)(3-1)1}) [\chi S]_{(4-2)(-4)2} \\ & - \frac{1}{16\pi(\omega_{4-2} + \omega_2 - \omega_4)} (S_{(4-2)2(-4)} + S_{2(4-2)(-4)}) [\chi S]_{(3-1)1(-3)}, \end{aligned} \quad (5.14)$$

and

$$\begin{aligned} T_{Res}^{(2)} = & \frac{1}{16\pi} \left(\frac{B_{(3-1)1(-3)}}{\omega_{3-1} + \omega_3 - \omega_1} [\chi S]_{(4-2)(-4)2} + \frac{B_{(4-2)(-4)2}}{\omega_{4-2} + \omega_2 - \omega_4} [\chi S]_{(3-1)1(-3)} \right) \\ & - \frac{1}{64\pi} \left(\frac{B_{1(-1-2)2}}{\omega_1 + \omega_2 - \omega_{1+2}} [\chi S]_{3(-3-4)4} + \frac{B_{3(-3-4)4}}{\omega_3 + \omega_4 - \omega_{3+4}} [\chi S]_{1(-1-2)2} \right), \end{aligned} \quad (5.15)$$

where we define

$$[\chi S]_{123} := B_{123} - S_{123} = \chi_{\mathcal{N}_\mu}(k_1, k_2, k_3)S_{123}. \quad (5.16)$$

Proof. The proof is similar to the proof of proposition 5.2 in [Appendix C](#). In particular, using the decomposition of $K^{(3)}$ given by terms (C1), we write

$$\{K^{(3)}, H_{Res}^{(3)}\} = \{K_0^{(3)}, H_{Res}^{(3)}\} + \{K_\chi^{(3)}, H_{Res}^{(3)}\}. \quad (5.17)$$

Then the first Poisson bracket leads to the coefficient (5.14), while the second bracket implies (5.15).

5.2. Modulational ansatz

We restrict ourselves to solutions in the form of near-monochromatic waves with carrier wavenumber $k_0 > 0$. For this purpose, we introduce the modulational ansatz

$$k = k_0 + \varepsilon\lambda, \quad \text{where } \frac{\lambda}{k_0} = O(1), \quad \varepsilon \ll 1, \quad (5.18)$$

and, accordingly, a function U is defined in the Fourier space as

$$U(\lambda) = z(k_0 + \varepsilon\lambda), \quad \bar{U}(\lambda) = \bar{z}(k_0 + \varepsilon\lambda), \quad (5.19a,b)$$

where the time dependence is omitted. In the physical space,

$$z(x) = \frac{1}{\sqrt{2\pi}} \int z(k) e^{ikx} dk = \frac{\varepsilon}{\sqrt{2\pi}} \int U(\lambda) e^{ik_0 x} e^{i\lambda \varepsilon x} d\lambda = \varepsilon u(X) e^{ik_0 x}, \quad (5.20)$$

where u , as a function of the long scale $X = \varepsilon x$, is the inverse Fourier transform of U . After the change of variables (5.18), the following integral identity for any function C holds:

$$\begin{aligned} & \int C(k_1, k_2, k_3, k_4) z_1 z_2 \bar{z}_3 \bar{z}_4 \delta_{1+2-3-4} dk_{1234} \\ &= \varepsilon^3 \int \tilde{C}(\lambda_1, \lambda_2, \lambda_3, \lambda_4) U_1 U_2 \bar{U}_3 \bar{U}_4 \delta_{1+2-3-4}^{(\lambda)} d\lambda_{1234}, \end{aligned} \quad (5.21)$$

where U_j stands for $U(\lambda_j)$, the Dirac distribution on the right-hand side is defined as $\delta_{1+2-3-4}^{(\lambda)} = (1/2\pi) \int \exp(-i(\lambda_1 + \lambda_2 - \lambda_3 - \lambda_4)X) dX$ and $C(k_1, k_2, k_3, k_4) = \tilde{C}(\lambda_1, \lambda_2, \lambda_3, \lambda_4)$.

5.3. Vanishing of the resonant cubic term $H_{Res}^{(3)}$

We show that, under the modulational regime (5.18), the resonant cubic Hamiltonian $H_{Res}^{(3)}$ given in (4.14) is sufficiently small and can be neglected. The estimates will be done for a cubic term of type

$$\mathcal{I} := \int T_{k_1, k_2, k_3} z_1 \bar{z}_2 z_3 \delta(k_1 - k_2 + k_3) dk_{123}, \quad (5.22)$$

which can be similarly repeated for each term of (4.14). After the change of variables (5.18), we have

$$\mathcal{I} = \frac{\varepsilon^3}{2\pi} \int e^{-ik_0 x} \int \tilde{T}_{\lambda_1, \lambda_2, \lambda_3} U_1 \bar{U}_2 U_3 \exp(-i(\lambda_1 - \lambda_2 + \lambda_3)(\varepsilon x)) d\lambda_{123} dx, \quad (5.23)$$

where $\tilde{T}_{\lambda_1, \lambda_2, \lambda_3} := T_{k_0 + \varepsilon\lambda_1, k_0 + \varepsilon\lambda_2, k_0 + \varepsilon\lambda_3}$. We identify the inner integral above with the function $f(\varepsilon x)$ as

$$f(\varepsilon x) := \int \tilde{T}_{\lambda_1, \lambda_2, \lambda_3} U_1 \bar{U}_2 U_3 \exp(-i(\lambda_1 - \lambda_2 + \lambda_3)(\varepsilon x)) d\lambda_{123}. \quad (5.24)$$

As a result, we have

$$\mathcal{I} = \frac{\varepsilon^3}{2\pi} \int e^{-ik_0 x} f(\varepsilon x) dx. \quad (5.25)$$

To show that the integral (5.25) is negligible, we use the scale-separation lemma 4.4 of Guyenne *et al.* (2022a).

5.4. Quartic interactions in the modulational regime

We approximate the coefficients in propositions 5.1 and 5.2 under the modulational regime (5.18).

LEMMA 5.4. *Under the modulational ansatz (5.18), we have*

$$\begin{aligned} & \int T_0 z_1 z_2 \bar{z}_3 \bar{z}_4 \delta_{1+2-3-4} dk_{1234} \\ &= \varepsilon^3 \int \left(c_0^l + \varepsilon c_0^r (\lambda_2 + \lambda_3) \right) U_1 U_2 \bar{U}_3 \bar{U}_4 \delta_{1+2-3-4}^{(\lambda)} d\lambda_{1234} + O(\varepsilon^5), \end{aligned} \quad (5.26)$$

where T_0 is given in proposition 5.1 and the coefficients are

$$\left. \begin{aligned} c_0^l &= \frac{k_0^3}{8\pi} + \frac{k_0^6}{16\pi\omega_0^2} \left(\frac{3}{2}\mathcal{P} - 5\mathcal{D}k_0^2 \right), \\ c_0^r &= \frac{3k_0^2}{16\pi} + \frac{k_0^6}{16\pi\omega_0^2} \left[\left(\frac{3}{2}\mathcal{P} - 5\mathcal{D}k_0^2 \right) \left(\frac{2}{k_0} + \frac{g + \mathcal{P}k_0^2 - 3\mathcal{D}k_0^4}{2\omega_0^2} \right) - 5\mathcal{D}k_0 \right]. \end{aligned} \right\} \quad (5.27)$$

Proof. The proof is based on the direct expansion of the coefficients (5.8) under the modulational regime (5.18) using the identities in (A1). For more detailed computations, we refer to the proof of lemma 5.2 in Guyenne *et al.* (2022b).

LEMMA 5.5. *Under the modulational ansatz (5.18), we have*

$$\begin{aligned} & \int T_{NoRes}^{(1)} z_1 z_2 \bar{z}_3 \bar{z}_4 \delta_{1+2-3-4} dk_{1234} \\ &= \varepsilon^3 \int \left(c_1^l + \varepsilon c_1^r (\lambda_2 + \lambda_3) \right) U_1 U_2 \bar{U}_3 \bar{U}_4 \delta_{1+2-3-4}^{(\lambda)} d\lambda_{1234} \\ &+ \frac{\varepsilon^4 k_0^2}{4\pi} \int |\lambda_1 - \lambda_3| U_1 U_2 \bar{U}_3 \bar{U}_4 \delta_{1+2-3-4}^{(\lambda)} d\lambda_{1234} + O(\varepsilon^5), \end{aligned} \quad (5.28)$$

$$\int T_{NoRes}^{(2)} z_1 z_2 \bar{z}_3 \bar{z}_4 \delta_{1+2-3-4} dk_{1234} = O(\varepsilon^5), \quad (5.29)$$

$$\begin{aligned} & \int T_{NoRes}^{(3)} z_1 z_2 \bar{z}_3 \bar{z}_4 \delta_{1+2-3-4} dk_{1234} \\ &= \varepsilon^3 \int (1 - \chi_{\mathcal{N}_\mu}(k_1, -k_1 - k_2, k_2)) (1 - \chi_{\mathcal{N}_\mu}(k_3, -k_3 - k_4, k_4)) \\ &\times \left(c_2^l + \varepsilon c_2^r (\lambda_2 + \lambda_3) \right) U_1 U_2 \bar{U}_3 \bar{U}_4 \delta_{1+2-3-4}^{(\lambda)} d\lambda_{1234} \\ &+ \frac{\varepsilon^4 k_0^2}{4\pi} \int (1 - \chi_{\mathcal{N}_\mu}(k_3 - k_1, k_1, -k_3)) (1 - \chi_{\mathcal{N}_\mu}(k_4 - k_2, -k_4, k_2)) \\ &\times (1 + \text{sgn}(\lambda_1 - \lambda_3)) |\lambda_1 - \lambda_3| U_1 U_2 \bar{U}_3 \bar{U}_4 \delta_{1+2-3-4}^{(\lambda)} d\lambda_{1234} + O(\varepsilon^5), \end{aligned} \quad (5.30)$$

where

$$\left. \begin{aligned}
c_1^l &= \frac{k_0^3 \omega_0^2}{4\pi \omega_{2k_0} (2\omega_0 + \omega_{2k_0})}, \\
c_1^r &= \frac{c_1^l}{2} \left(\frac{3g - 5\mathcal{P}k_0^2 + 7\mathcal{D}k_0^4}{\omega_0^2} + \frac{g + 4\mathcal{P}k_0^2 - 48\mathcal{D}k_0^4}{\omega_{2k_0}^2} \right. \\
&\quad \left. - \frac{g - 12\mathcal{P}k_0^2 + 80\mathcal{D}k_0^4}{\omega_{2k_0} (2\omega_0 + \omega_{2k_0})} - \frac{g - 3\mathcal{P}k_0^2 + 5\mathcal{D}k_0^4}{\omega_0 (2\omega_0 + \omega_{2k_0})} \right), \\
c_2^l &= -\frac{k_0^3 \omega_0^2}{4\pi \omega_{2k_0} (2\omega_0 - \omega_{2k_0})}, \\
c_2^r &= \frac{c_2^l}{2} \left(\frac{3g - 5\mathcal{P}k_0^2 + 7\mathcal{D}k_0^4}{\omega_0^2} + \frac{g + 4\mathcal{P}k_0^2 - 48\mathcal{D}k_0^4}{\omega_{2k_0}^2} \right. \\
&\quad \left. + \frac{g - 12\mathcal{P}k_0^2 + 80\mathcal{D}k_0^4}{\omega_{2k_0} (2\omega_0 - \omega_{2k_0})} - \frac{g - 3\mathcal{P}k_0^2 + 5\mathcal{D}k_0^4}{\omega_0 (2\omega_0 - \omega_{2k_0})} \right).
\end{aligned} \right\} \quad (5.31)$$

Proof. The proof is presented in [Appendix D](#).

LEMMA 5.6. *Under the modulational ansatz (5.18), we have*

$$\begin{aligned}
&\int T_{Res} z_1 z_2 \bar{z}_3 \bar{z}_4 \delta_{1+2-3-4} dk_{1234} \\
&= \frac{\varepsilon^4 k_0^2}{8\pi} \int [\chi_{\mathcal{N}_\mu}(k_3 - k_1, k_1, -k_3) + \chi_{\mathcal{N}_\mu}(k_4 - k_2, -k_4, k_2) \\
&\quad - 2\chi_{\mathcal{N}_\mu}(k_3 - k_1, k_1, -k_3)\chi_{\mathcal{N}_\mu}(k_4 - k_2, -k_4, k_2)] \\
&\quad \times (1 + \text{sgn}(\lambda_1 - \lambda_3)) |\lambda_1 - \lambda_3| U_1 U_2 \bar{U}_3 \bar{U}_4 \delta_{1+2-3-4}^{(\lambda)} d\lambda_{1234} \\
&+ \frac{\varepsilon^3}{2} \int [\chi_{\mathcal{N}_\mu}(k_1, -k_1 - k_2, k_2) + \chi_{\mathcal{N}_\mu}(k_3, -k_3 - k_4, k_4) \\
&\quad - 2\chi_{\mathcal{N}_\mu}(k_1, -k_1 - k_2, k_2)\chi_{\mathcal{N}_\mu}(k_3, -k_3 - k_4, k_4)] \\
&\quad \times (c_2^l + \varepsilon c_2^r(\lambda_2 + \lambda_3)) U_1 U_2 \bar{U}_3 \bar{U}_4 \delta_{1+2-3-4}^{(\lambda)} d\lambda_{1234}. \quad (5.32)
\end{aligned}$$

Proof. The proof can be found in [Appendix E](#).

Based on lemmas 5.4–5.6, the reduced Hamiltonian $H_+^{(4)}$ has the form

$$\begin{aligned}
H_+^{(4)} &= \varepsilon^3 \int \frac{\alpha}{4\pi} U_1 U_2 \bar{U}_3 \bar{U}_4 \delta_{1+2-3-4}^{(\lambda)} d\lambda_{1234} \\
&+ \varepsilon^4 \int \left(\frac{\beta}{8\pi} (\lambda_2 + \lambda_3) - \frac{k_0^2}{8\pi} \gamma |\lambda_1 - \lambda_3| \right) U_1 U_2 \bar{U}_3 \bar{U}_4 \delta_{1+2-3-4}^{(\lambda)} d\lambda_{1234} + O(\varepsilon^5), \quad (5.33)
\end{aligned}$$

where, using $k_j = k_0 + \varepsilon \lambda_j$ from (5.18), we denote

$$\frac{\alpha}{4\pi} := c_0^l - \frac{1}{2}c_1^l - \frac{1}{2} [1 - \chi_{\mathcal{N}_\mu}(k_1, -k_1 - k_2, k_2)\chi_{\mathcal{N}_\mu}(k_3, -k_3 - k_4, k_4)] c_2^l, \quad (5.34)$$

$$\frac{\beta}{8\pi} := c_0^r - \frac{1}{2}c_1^r - \frac{1}{2} [1 - \chi_{\mathcal{N}_\mu}(k_1, -k_1 - k_2, k_2)\chi_{\mathcal{N}_\mu}(k_3, -k_3 - k_4, k_4)] c_2^r \quad (5.35)$$

and

$$\gamma = 1 + [1 - \chi_{\mathcal{N}_\mu}(k_3 - k_1, k_1, -k_3)\chi_{\mathcal{N}_\mu}(k_4 - k_2, -k_4, k_2)] (1 + \text{sgn}(\lambda_1 - \lambda_3)). \quad (5.36)$$

6. Hamiltonian Dysthe equation

From the expressions (5.34)–(5.36), it is clear that the coefficients in the Hamiltonian (5.33) depend on k_0 via (5.27) and (5.31), and on the characteristic function at corresponding points inside the integral. In turn, the choices of μ in the definition of $\chi_{\mathcal{N}_\mu}$ in (3.29) and of k_0 in our modulational ansatz (5.18) affect the evaluation of these characteristic functions. We concentrate on two examples of values for k_0 , motivated by the three-wave resonant curve (figure 2) and the numerical simulations validating our asymptotics in §7. We choose $k_0 = 0.9$ and $k_0 = 2$, which lead to different values of characteristic functions appearing in (5.34)–(5.36). In both cases, we set $\mu = O(\varepsilon)$. Details are given in the next subsection.

6.1. Explicit formulae for α , β and γ

6.1.1. Case $k_0 = 0.9$

Based on the construction of the neighbourhood around the resonant set in (3.28), we have the following identities:

$$\chi_{\mathcal{N}_\mu}(k_1, -k_1 - k_2, k_2) = 0, \quad (6.1)$$

and

$$\chi_{\mathcal{N}_\mu}(k_4 - k_2, -k_4, k_2) = 0 \quad \text{whenever } \text{sgn}(k_4 - k_2) = +1. \quad (6.2)$$

The validity of (6.1) follows from (5.18) and the choice $\mu = O(\varepsilon)$:

$$\begin{aligned} (k_1, k_2) \in \mathcal{B}_c(k_0) &:= \{(x, y) : x = k_0 + O(\varepsilon), y = k_0 + O(\varepsilon)\} \not\subseteq \mathcal{C}_\mu \\ &\implies (k_1, -k_1 - k_2, k_2) \notin \mathcal{N}_\mu. \end{aligned} \quad (6.3)$$

As for (6.2), under (5.18), we have $k_4 - k_2 = \varepsilon(\lambda_4 - \lambda_2) = O(\varepsilon)$ and $k_2 = k_0 + \varepsilon \lambda_2$. Then, if $k_4 - k_2 > 0$, the points $(k_4 - k_2, k_2)$ are located far away from the set \mathcal{C}_μ^+ and so

$$\begin{aligned} (k_4 - k_2, k_2) \in \mathcal{B}_s(k_0) &:= \{(x, y) : 0 \leq x \leq O(\varepsilon), y = k_0 + O(\varepsilon)\} \not\subseteq \mathcal{C}_\mu^+ \\ &\implies (k_4 - k_2, -k_4, k_2) \notin \mathcal{N}_\mu. \end{aligned} \quad (6.4)$$

As a result, the coefficients in (5.34)–(5.36) reduce to

$$\frac{\alpha}{4\pi} = c_0^l - \frac{1}{2}(c_1^l + c_2^l), \quad \frac{\beta}{8\pi} = c_0^r - \frac{1}{2}(c_1^r + c_2^r), \quad \gamma = 2 + \text{sgn}(\lambda_1 - \lambda_3). \quad (6.5a-c)$$

When substituting γ into the integral (5.33), the term $\text{sgn}(\lambda_1 - \lambda_3)$ will disappear since

$$\begin{aligned} & \int \text{sgn}(\lambda_1 - \lambda_3) |\lambda_1 - \lambda_3| U_1 U_2 \bar{U}_3 \bar{U}_4 \delta_{1+2-3-4}^{(\lambda)} d\lambda_{1234} \\ &= \int (\lambda_1 - \lambda_3) U_1 U_2 \bar{U}_3 \bar{U}_4 \delta_{1+2-3-4}^{(\lambda)} d\lambda_{1234} \\ &= \frac{1}{2} \int (\lambda_1 + \lambda_2 - \lambda_3 - \lambda_4) U_1 U_2 \bar{U}_3 \bar{U}_4 \delta_{1+2-3-4}^{(\lambda)} d\lambda_{1234} = 0, \end{aligned} \quad (6.6)$$

where we have used the index rearrangement $(\lambda_1, \lambda_2, \lambda_3, \lambda_4) \rightarrow (\lambda_2, \lambda_1, \lambda_3, \lambda_4)$ and the delta condition $\lambda_1 + \lambda_2 - \lambda_3 - \lambda_4 = 0$. As a consequence, we will simply write $\gamma = 2$ in this case.

6.1.2. Case $k_0 = 2$

If k_0 is sufficiently large, we have

$$\chi_{\mathcal{N}_\mu}(k_1, -k_1 - k_2, k_2) = 0, \quad (6.7)$$

and

$$\chi_{\mathcal{N}_\mu}(k_4 - k_2, -k_4, k_2) = 1 \quad \text{whenever } \text{sgn}(k_4 - k_2) = +1. \quad (6.8)$$

Equation (6.7) holds due to estimates similar to (6.3). Equation (6.8) is different from (6.2) since, for a sufficiently large value of k_0 , the points $(k_4 - k_2, k_2)$ are located inside the set \mathcal{C}_μ^+ ,

$$\begin{aligned} (k_4 - k_2, k_2) &\in \{(x, y) : 0 \leq x \leq O(\varepsilon), y = k_0 + O(\varepsilon)\} \subset \mathcal{C}_\mu^+ \\ \implies (k_4 - k_2, -k_4, k_2) &\in \mathcal{N}_\mu, \end{aligned} \quad (6.9)$$

and we get

$$\frac{\alpha}{4\pi} = c_0^l - \frac{1}{2}(c_1^l + c_2^l), \quad \frac{\beta}{8\pi} = c_0^r - \frac{1}{2}(c_1^r + c_2^r), \quad \gamma = 1. \quad (6.10a-c)$$

Figure 4 shows the location of points (k_1, k_2) and $(k_4 - k_2, k_2)$ with $k_4 - k_2 > 0$ for $k_0 = 0.9$ (figure 4a) and $k_0 = 2$ (figure 4b) relative to the neighbourhood \mathcal{C}_μ . In figure 4(a) for $k_0 = 0.9$, Box 1 represents the set $\mathcal{B}_s(k_0)$ of all possible values of $(k_4 - k_2, k_2)$ with $k_4 - k_2 > 0$ under the modulational ansatz (5.18), according to (6.4). Box 2 represents the set $\mathcal{B}_c(k_0)$ in (6.3). Similar sets are depicted in figure 4(b) for $k_0 = 2$.

6.2. Derivation of the Dysthe equation

The third-order normal form transformation has eliminated all cubic terms from the Hamiltonian H . In the modulational regime (5.18), the reduced Hamiltonian (now denoted by H) is

$$H = H^{(2)} + H_+^{(4)}, \quad (6.11)$$

up to fourth order. In the physical variables (u, \bar{u}) , it reads

$$\begin{aligned} H &= \varepsilon \int \bar{u} \omega(k_0 + \varepsilon D_X) u dX + \varepsilon^3 \frac{\alpha}{2} \int |u|^4 dX \\ &+ \varepsilon^4 \frac{\beta}{2} \int |u|^2 \text{Im}(\bar{u} \partial_X u) dX - \varepsilon^4 \frac{\gamma k_0^2}{4} \int |u|^2 |D_X| |u|^2 dX + O(\varepsilon^5), \end{aligned} \quad (6.12)$$

where $D_X = -i \partial_X$ for the slow spatial variable X (so that its Fourier symbol is λ) and accordingly $|D_X|$ is the non-local operator whose Fourier symbol is $|\lambda|$. Expanding the

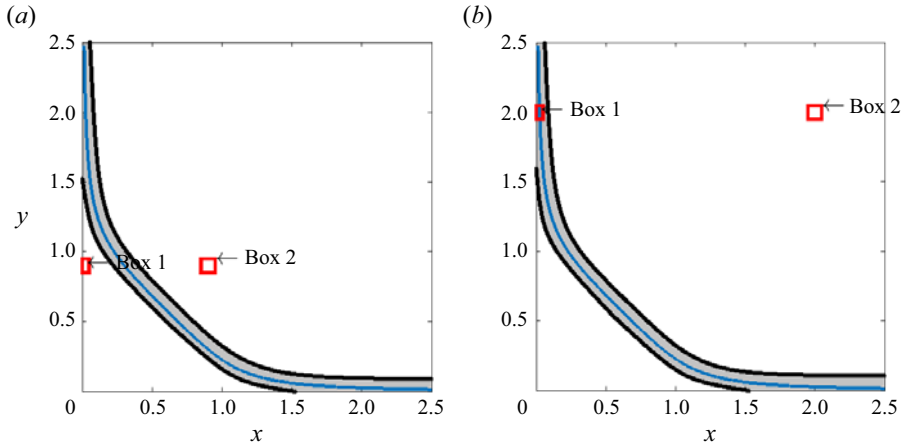


Figure 4. Location of points (k_1, k_2) and $(k_4 - k_2, k_2)$ with $k_4 - k_2 > 0$ relative to the neighbourhood \mathcal{C}_μ , in the case (a) $k_0 = 0.9$ and (b) $k_0 = 2$ for $\mathcal{P} = 1$. Box 1 represents the set $\mathcal{B}_s(k_0)$ and Box 2 represents the set $\mathcal{B}_c(k_0)$.

linear dispersion relation in (6.12) around k_0 as

$$\omega(k_0 + \varepsilon D_X) = \omega_0 + \varepsilon \omega'_0 D_X + \frac{1}{2} \varepsilon^2 \omega''_0 D_X^2 + \frac{1}{6} \varepsilon^3 \omega'''_0 D_X^3 + O(\varepsilon^4), \quad (6.13)$$

gives an alternate form of the Hamiltonian H in physical variables

$$H = \int \left[\varepsilon \omega_0 |u|^2 + \varepsilon^2 \omega'_0 \text{Im}(\bar{u} \partial_X u) + \frac{1}{2} \varepsilon^3 \omega''_0 |\partial_X u|^2 + \frac{1}{2} \varepsilon^3 \alpha |u|^4 - \frac{1}{6} \varepsilon^4 \omega'''_0 \text{Im}(\bar{u} \partial_X^3 u) + \frac{1}{2} \varepsilon^4 \beta |u|^2 \text{Im}(\bar{u} \partial_X u) - \frac{1}{4} \varepsilon^4 \gamma k_0^2 |u|^2 |D_X| |u|^2 \right] dX + O(\varepsilon^5). \quad (6.14)$$

Coefficients in (6.13) have the following expressions:

$$\left. \begin{aligned} \omega'_0 &:= \partial_k \omega(k_0) = \frac{g + 5\mathcal{D}k_0^4 - 3\mathcal{P}k_0^2}{2\omega_0}, \\ \omega''_0 &:= \partial_k^2 \omega(k_0) = \frac{15\mathcal{D}^2 k_0^8 - 22\mathcal{D}\mathcal{P}k_0^6 + 30g\mathcal{D}k_0^4 + 3\mathcal{P}^2 k_0^4 - 6g\mathcal{P}k_0^2 - g^2}{4\omega_0^{3/2}}, \\ \omega'''_0 &:= \partial_k^3 \omega(k_0) = 3 \left(5\mathcal{D}^3 k_0^{12} - 13\mathcal{D}^2 \mathcal{P}k_0^{10} - 5g\mathcal{D}^2 k_0^8 + 15\mathcal{D}\mathcal{P}^2 k_0^8 \right. \\ &\quad \left. - 34g\mathcal{D}\mathcal{P}k_0^6 + \mathcal{P}^3 k_0^6 + 55g^2 \mathcal{D}k_0^4 - 5g\mathcal{P}^2 k_0^4 - 5g^2 \mathcal{P}k_0^2 + g^3 \right) / \left(8\omega_0^{5/2} \right). \end{aligned} \right\} \quad (6.15)$$

The Hamiltonian system

$$\partial_t \begin{pmatrix} u \\ \bar{u} \end{pmatrix} = \varepsilon^{-1} \begin{pmatrix} 0 & -i \\ i & 0 \end{pmatrix} \begin{pmatrix} \partial_u H \\ \partial_{\bar{u}} H \end{pmatrix}, \quad (6.16)$$

implies

$$\begin{aligned} i\partial_t u &= \varepsilon^{-1}\partial_u H, \\ &= \omega_0 u - i\varepsilon\omega'_0\partial_X u - \frac{1}{2}\varepsilon^2\omega''_0\partial_X^2 u + \varepsilon^2\alpha|u|^2 u \\ &\quad + \frac{i}{6}\varepsilon^3\omega'''_0\partial_X^3 u - i\varepsilon^3\beta|u|^2\partial_X u - \varepsilon^3\frac{\gamma k_0^2}{2}u|D_X||u|^2, \end{aligned} \quad (6.17)$$

which is a Hamiltonian Dysthe equation for two-dimensional hydroelastic waves on deep water. It describes modulated waves moving in the positive x -direction at group speed ω'_0 as shown by the advection term. The non-local term $u|D_X||u|^2$, a signature of the Dysthe equation, reflects the presence of the wave-induced mean flow as in the classical derivation using the method of multiple scales. The coefficient of this mean-flow term is similar to that in the pure gravity case ($\mathcal{D} = 0, \mathcal{P} = 0$) except for the dependence on γ .

The first two terms on the right-hand side of (6.17) can be eliminated via phase invariance and reduction to a moving reference frame. The latter is equivalent, in the framework of canonical transformations, to subtraction from H of a multiple of the momentum (2.10) which reduces to

$$I = \int \eta(\partial_x \xi) dx = \int [k_0|u|^2 + \varepsilon \operatorname{Im}(\bar{u}\partial_X u)] dX, \quad (6.18)$$

while the former is equivalent to subtraction from H of a multiple of the wave action

$$M = \varepsilon \int |u|^2 dX, \quad (6.19)$$

which is conserved due to the phase-invariance property of the Dysthe equation. The resulting Hamiltonian is given by

$$\hat{H} = H - \varepsilon\omega'_0 I - (\omega_0 - k_0\omega'_0)M, \quad (6.20)$$

which, after introducing a new long-time scale $\tau = \varepsilon^2 t$, leads to the following version of the Hamiltonian Dysthe equation:

$$i\partial_\tau u = -\frac{1}{2}\omega''_0\partial_X^2 u + \alpha|u|^2 u + \frac{i}{6}\varepsilon\omega'''_0\partial_X^3 u - i\varepsilon\beta|u|^2\partial_X u - \varepsilon\frac{\gamma k_0^2}{2}u|D_X||u|^2. \quad (6.21)$$

REMARK 6.1. *The Hamiltonian Dysthe equation derived by Craig et al. (2021a) for two-dimensional deep-water surface gravity waves ($\mathcal{D} = 0, \mathcal{P} = 0$) reads*

$$i\partial_\tau u = \frac{g}{8\omega_0^3}\partial_X^2 u + k_0^3|u|^2 u + i\varepsilon\frac{g^3}{16\omega_0^5}\partial_X^3 u - 3i\varepsilon k_0^2|u|^2\partial_X u - \varepsilon k_0^2 u|D_X||u|^2. \quad (6.22)$$

It is natural to expect that, in the limit $\mathcal{D} \rightarrow 0$ and $\mathcal{P} \rightarrow 0$, the coefficients of (6.21) converge to those of (6.22). Indeed, a direct computation verifies this convergence for the coefficients of the linear terms as well as $\alpha \rightarrow k_0^3$, $\beta \rightarrow 3k_0^2$ together with $\gamma \rightarrow 2$ for any k_0 because resonant triads are ruled out in this situation, hence $\chi_{\mathcal{N}_\mu} = 0$.

REMARK 6.2. *We have checked that the coefficients ω''_0 and α in the NLS part of (6.17) coincide with those of the NLS equation proposed by Trichtchenko et al. (2019) for g , $\mathcal{D} \neq 0$, and by Slunyaev & Stepanyants (2022) for g , $\mathcal{P} \neq 0$. Trichtchenko et al. (2019) employed the same Cosserat model (2.5) for ice bending but ignored ice compression. Slunyaev & Stepanyants (2022) examined ice bending and compression but they considered a non-Hamiltonian KL-type model for ice bending.*

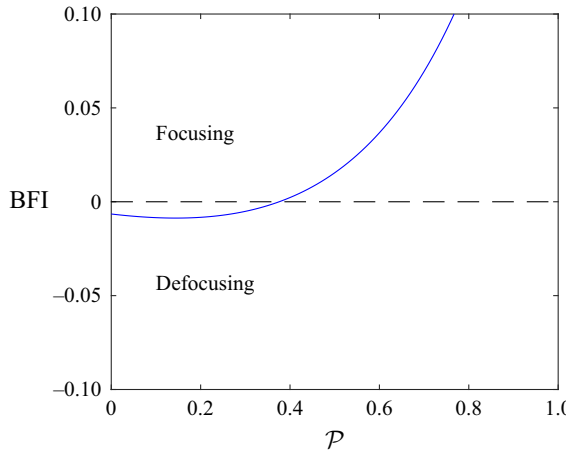


Figure 5. The BF instability/stability criterion at k_{min} for the NLS equation as a function of \mathcal{P} .

6.3. Envelope solitons

We take this opportunity to highlight a salient effect of ice compression when added to ice bending. As analysed by Akylas (1983), a general result about the NLS equation in the focusing regime is that it admits permanent envelope solitons (i.e. solitary wave packets) provided that $c = c_g$ is realized in the wave system. If so, the wave packet has carrier wavenumber k_{min} and propagates in such a way that its crests are stationary relative to its envelope.

In the flexural-gravity case ($\mathcal{P} = 0$), it has been revealed that such envelope solitons do not exist (Milewski *et al.* 2011; Guyenne & Părău 2012), i.e. the corresponding NLS equation is of defocusing type because of the sign of the Benjamin–Feir index (BFI) defined as the product of the dispersion coefficient ω_0'' and the coefficient of the cubic term α , namely

$$\text{BFI} = -\omega_0''\alpha = -0.006 < 0, \quad \text{at } k = k_{min} = 0.76, \quad (6.23)$$

according to the Benjamin–Feir (BF) criterion for modulational instability, and with k_{min} defined by (3.32). On the other hand, we get

$$\text{BFI} = -\omega_0''\alpha = 0.2954 > 0, \quad \text{at } k = k_{min} = 0.88, \quad (6.24)$$

for $\mathcal{P} = 1$, which implies a focusing regime. Figure 5 portrays BFI for k_{min} as a function of \mathcal{P} . As explained earlier, we restrict ourselves to the interval $0 \leq \mathcal{P} < 2$ where non-conservative exponential wave growth/decay is ruled out. We find that the change from defocusing to focusing occurs around $\mathcal{P} = 0.39$ after which BFI quickly increases. This regime transition is significant, varying from negative BFI of low magnitude to positive BFI of high magnitude over a relatively short interval of \mathcal{P} . For example, if $\mathcal{P} = 1.9$, the much larger value of $\text{BFI} \simeq 55$ is beyond the range displayed in this figure.

7. Numerical results

We show numerical simulations to illustrate the performance of our Hamiltonian Dysthe equation. We consider the modulational instability of Stokes waves in the presence of sea ice and examine the influence of ice compression. We compare these results with predictions by the cubic NLS model and to direct simulations of the full Euler system.

We also test the capability of our reconstruction procedure against a more conventional approach.

7.1. Stability of Stokes waves

We first give the theoretical prediction for modulational or BF instability of Stokes waves in sea ice. These are represented in (6.17) by the exact uniform solution

$$u_0(t) = B_0 \exp(-i(\omega_0 + \varepsilon^2 \alpha B_0^2)t), \quad (7.1)$$

where B_0 is a positive real constant. In the gravity water wave case ($\mathcal{D} = 0$, $\mathcal{P} = 0$), such a solution is known to be linearly unstable with respect to sideband (i.e. long-wave) perturbations.

The formal calculation consists in linearizing (6.17) about u_0 by inserting a perturbation of the form

$$u(X, t) = u_0(t) [1 + B(X, t)], \quad (7.2)$$

where

$$B(X, t) = B_1 e^{\Omega t + i\lambda X} + B_2 e^{\bar{\Omega}t - i\lambda X}, \quad (7.3)$$

and B_1, B_2 are complex coefficients. We find that the condition $\text{Re}(\Omega) \neq 0$ for instability implies

$$\alpha_1 = -\frac{\omega_0''}{2} \lambda^2 \left[2B_0^2 \left(\alpha - \varepsilon \frac{\gamma k_0^2}{2} |\lambda| \right) + \frac{\omega_0''}{2} \lambda^2 \right] > 0. \quad (7.4)$$

This is a tedious but straightforward calculation for which we omit the details (Craig *et al.* 2021a; Guyenne *et al.* 2022b).

In view of the subsequent comparison with numerical simulations of the Euler system, all variables associated with the envelope model are now rescaled to absorb ε back into their definition. Figure 6 depicts the normalized growth rate

$$\frac{|\text{Re}(\Omega)|}{\omega_0} = \frac{\sqrt{\alpha_1}}{\omega_0}, \quad (7.5)$$

delimiting the instability region as predicted by condition (7.4) for $(A_0, k_0) = (0.1, 0.9)$ and $(0.01, 5)$ with varying values of \mathcal{P} . These parameter regimes are representative of the two different cases $\gamma = 2$ and 1 for the mean-flow term, as discussed in § 6.1. They correspond to initial wave steepness $\varepsilon = k_0 A_0 = 0.09$ and 0.05, respectively. Note that the envelope amplitude B_0 and the surface amplitude A_0 are related by

$$B_0 = A_0 \sqrt{\frac{\omega_0}{2k_0}}, \quad (7.6)$$

according to (2.25) and (5.20).

We see in figure 6 that instability tends to be enhanced with increasing \mathcal{P} . The growth rate is especially strong for $(A_0, k_0) = (0.1, 0.9)$ and $\mathcal{P} = 1.9$. By contrast, the variations in \mathcal{P} are weaker for $(A_0, k_0) = (0.01, 5)$. Maximum growth rate occurs around $\lambda = 0.02$ for $(A_0, k_0) = (0.1, 0.9)$ and around $\lambda = 0.1$ for $(A_0, k_0) = (0.01, 5)$. The wavenumber at maximum growth rate (as well as the extent of the instability region) differs by an order of magnitude between these two configurations.

The same remark can be made when comparing these results with predictions on BF instability for the gravity water wave problem with similar values of ε (Craig *et al.* 2021a;

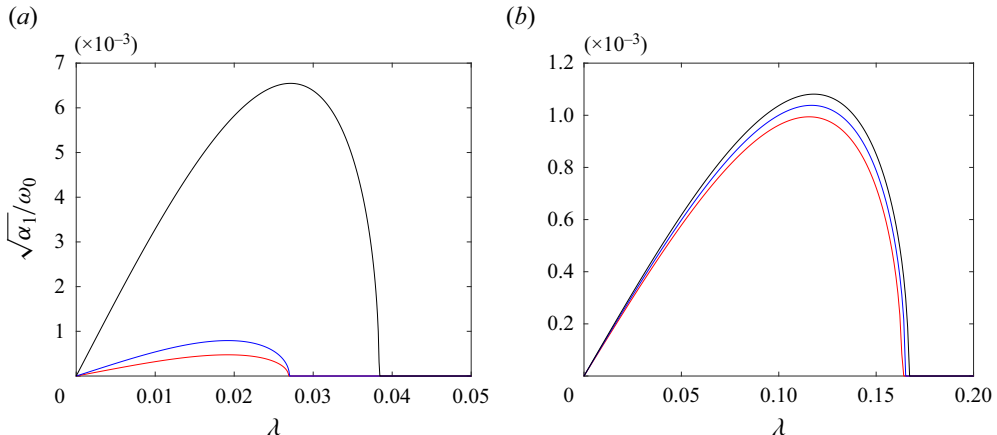


Figure 6. Regions of BF instability according to (7.4) for (a) $(A_0, k_0) = (0.1, 0.9)$ and (b) $(A_0, k_0) = (0.01, 5)$. The various curves represent $\mathcal{P} = 0$ (red), $\mathcal{P} = 1$ (blue), $\mathcal{P} = 1.9$ (black).

Guyenne *et al.* 2022b). Including elasticity leads to narrower regions of instability centred around smaller sideband wavenumbers λ , which are smaller by orders of magnitude than their counterparts in the pure gravity case. This implies that a much longer domain is needed in the present simulations to observe this instability with such long-wave modulations.

7.2. Reconstruction of the original variables

At any instant t , the surface elevation and velocity potential can be reconstructed from the wave envelope by inverting the normal form transformation. This is accomplished by solving the auxiliary system backward from $s = 0$ to $s = -1$, with ‘initial’ conditions given by the transformed variables

$$\eta(x, t)|_{s=0} = \frac{1}{\sqrt{2}} a^{-1}(D) \left[u(x, t) e^{ik_0 x} + \bar{u}(x, t) e^{-ik_0 x} \right], \quad (7.7)$$

$$\xi(x, t)|_{s=0} = \frac{1}{i\sqrt{2}} a(D) \left[u(x, t) e^{ik_0 x} - \bar{u}(x, t) e^{-ik_0 x} \right], \quad (7.8)$$

according to (2.25) and (5.20). In these expressions, u obeys (6.17) and $a^{-1}(D) = \sqrt{|D|/\omega(D)}$. The final solution at $s = -1$ represents the original variables (η, ξ) . During the evolution in s , higher-order harmonic contributions to (η, ξ) are produced by the nonlinear terms in (4.20a,b) starting from the first harmonics (7.7)–(7.8) associated with carrier wavenumber k_0 .

7.3. Simulations

We test this Hamiltonian Dysthe equation against the full equations (2.8) in the context of BF instability of Stokes waves in sea ice. Following a high-order spectral approach (Craig & Sulem 1993; Guyenne & Päräu 2012), (2.8) are discretized in space by a pseudospectral method via the fast Fourier transform (FFT). Nonlinear products are calculated in the physical space, while Fourier multipliers and spatial derivatives are evaluated in the Fourier space. The computational domain is set to $0 \leq x < L$ with periodic boundary

conditions and is divided into a regular mesh of N collocation points. Both functions η and ξ are expressed in terms of truncated Fourier series

$$\begin{pmatrix} \eta(x_j, t) \\ \xi(x_j, t) \end{pmatrix} = \sum_{p=-N/2}^{N/2-1} \begin{pmatrix} \hat{\eta}_p(t) \\ \hat{\xi}_p(t) \end{pmatrix} e^{i \kappa_p x_j}, \quad \kappa_p = p \Delta \kappa, \quad x_j = j \Delta x, \quad j = 0, \dots, N-1, \quad (7.9)$$

where $\Delta \kappa = 2\pi/L$ and $\Delta x = L/N$. Note that $\{\kappa_p\}$ represents the set of discrete values associated with any wavenumber $k_\ell \in \mathbb{R}$. The DNO is approximated by its series expansion (2.16) for which a small number M of terms is sufficient to achieve highly accurate results in light of its analyticity properties. The value $M = 6$ is selected based on previous extensive tests (Xu & Guyenne 2009). Time integration of (2.8) is carried out in the Fourier space so that linear terms can be solved exactly by the integrating factor technique. The nonlinear terms are integrated in time by using a fourth-order Runge–Kutta scheme with constant step Δt . More details can be found in Guyenne & Pärä (2012) and Xu & Guyenne (2009), with the exception that (2.8) for $\mathbf{v} = (\eta, \xi)^\top$ can be written as

$$\partial_t \mathbf{v} = \mathbf{L}\mathbf{v} + \mathbf{N}(\mathbf{v}), \quad (7.10)$$

where the linear part $\mathbf{L}\mathbf{v}$ is defined by

$$\mathbf{L}\mathbf{v} = \begin{pmatrix} 0 & G^{(0)} \\ -g - \mathcal{D}\partial_x^4 - \mathcal{P}\partial_x^2 & 0 \end{pmatrix} \begin{pmatrix} \eta \\ \xi \end{pmatrix}, \quad (7.11)$$

and the nonlinear part $\mathbf{N}(\mathbf{v}) = (N_1, N_2)^\top$ is given by

$$N_1 = G(\eta) - G^{(0)}, \quad (7.12)$$

$$\begin{aligned} N_2 = & -\frac{1}{2}(\partial_x \xi)^2 + \frac{1}{2} \frac{[G(\eta)\xi + (\partial_x \eta)(\partial_x \xi)]^2}{1 + (\partial_x \eta)^2} \\ & - \mathcal{D} \left(\partial_s^2 \kappa - \partial_x^4 \eta + \frac{1}{2} \kappa^3 \right) - \mathcal{P}(\kappa - \partial_x^2 \eta). \end{aligned} \quad (7.13)$$

In the Fourier space, the integrating factor $\Theta_k(t)$ associated with $\mathbf{L}\mathbf{v}$ takes the form

$$\Theta_k(t) = \begin{pmatrix} \cos(\omega_k t) & \sqrt{\frac{G^{(0)}}{g + \mathcal{D}k^4 - \mathcal{P}k^2}} \sin(\omega_k t) \\ -\sqrt{\frac{g + \mathcal{D}k^4 - \mathcal{P}k^2}{G^{(0)}}} \sin(\omega_k t) & \cos(\omega_k t) \end{pmatrix}, \quad (7.14)$$

for $k \neq 0$, and

$$\Theta_0(t) = \begin{pmatrix} 1 & 0 \\ -gt & 1 \end{pmatrix}, \quad (7.15)$$

for $k = 0$ according to l'Hôpital's rule. The resulting fourth-order Runge–Kutta scheme reads

$$f_1 = N_k(\mathbf{v}_k^n), \quad (7.16)$$

$$f_2 = \Theta_k\left(-\frac{\Delta t}{2}\right)N_k\left[\Theta_k\left(\frac{\Delta t}{2}\right)\left(\mathbf{v}_k^n + \frac{\Delta t}{2}f_1\right)\right], \quad (7.17)$$

$$f_3 = \Theta_k\left(-\frac{\Delta t}{2}\right)N_k\left[\Theta_k\left(\frac{\Delta t}{2}\right)\left(\mathbf{v}_k^n + \frac{\Delta t}{2}f_2\right)\right], \quad (7.18)$$

$$f_4 = \Theta_k(-\Delta t)N_k\left[\Theta_k(\Delta t)\left(\mathbf{v}_k^n + \Delta t f_3\right)\right], \quad (7.19)$$

$$\mathbf{v}_k^{n+1} = \Theta_k(\Delta t)\mathbf{v}_k^n + \frac{\Delta t}{6}\Theta_k(\Delta t)(f_1 + 2f_2 + 2f_3 + f_4), \quad (7.20)$$

for the solution $\mathbf{v}_k = (\eta_k, \xi_k)^\top$ advancing from time t_n to time $t_{n+1} = t_n + \Delta t$.

The same numerical methods are used to solve the envelope equation (6.17), with the same resolutions in space and time. On the other hand, for the reconstruction procedure, the Fourier integrals in the auxiliary system are not evaluated by a pseudospectral method with the FFT because they cannot be expressed in terms of convolution integrals, unlike the case of surface gravity waves (Craig *et al.* 2021a; Guyenne *et al.* 2022a). A reason is the more complicated expression of the linear dispersion relation in this problem due to ice bending and compression, which does not allow for further simplification of the interaction kernels in (4.20a,b). Instead, these Fourier integrals are computed by direct quadrature. More specifically, they are reduced to one-dimensional integrals in k_1 (or k_2) by integrating out the Dirac delta functions before applying the trapezoidal rule. The interval of integration as well as all Fourier coefficients in the integrands are confined to the truncated spectrum $-N/2 \leq p \leq N/2 - 1$ by virtue of (7.9). The coupled system (4.20a,b) is evolved in s via a fourth-order Runge–Kutta scheme, with step size $\Delta s = 10\Delta t$ or $100\Delta t$. By construction, (4.20a,b) are purely nonlinear (i.e. quadratic in nonlinearity) and do not contain any stiff linear terms. Accordingly, the value of Δs may be selected so that $0 < \Delta t \ll \Delta s \ll 1$, which helps speed up the s -marching process to mitigate the computational cost entailed by the quadrature rule. We have checked that using a smaller value of Δs (say $\Delta s = \Delta t$) gives similar results.

While the FFT cannot be exploited for the reconstruction procedure, direct quadrature of the Fourier integrals in (4.20a,b) was not found to be a major issue in this two-dimensional setting. Because this computation is not performed at each instant t (only when data are recorded) and because it is performed over a short interval $-1 \leq s \leq 0$, the associated cost is insignificant overall. We point out again that (4.20a,b) are an exact representation of the normal form transformation to eliminate non-resonant cubic interactions in this problem. They are solved numerically in their full form, without resorting to any asymptotic approximation. Indetermination due to a_1^2 or a_3^2 being singular at $k_1 = 0$ or $k_3 = 0$ in P_{123} and Q_{123} may be lifted by simply setting the corresponding contributions to zero by virtue of the zero-mass assumption. Because wavenumbers are discrete in this numerical context and to accommodate floating-point arithmetic, the characteristic function $\chi_{\mathcal{N}}(k_1, k_2, k_3)$ in (4.17) is implemented under relaxed conditions

$$\chi_{\mathcal{N}}(k_1, k_2, k_3) = \begin{cases} 1, & \text{if } k_1 + k_2 + k_3 = 0, \quad |\omega_1 - \omega_2 + \omega_3| < \Delta, \\ 0, & \text{otherwise,} \end{cases} \quad (7.21)$$

with $0 < \Delta \ll 1$. We have tested different values of Δ , i.e. $\Delta = \{10^{-12}, 10^{-6}, 10^{-2}\}$ and obtained similar results, which suggests that such a resonant triad does not contribute

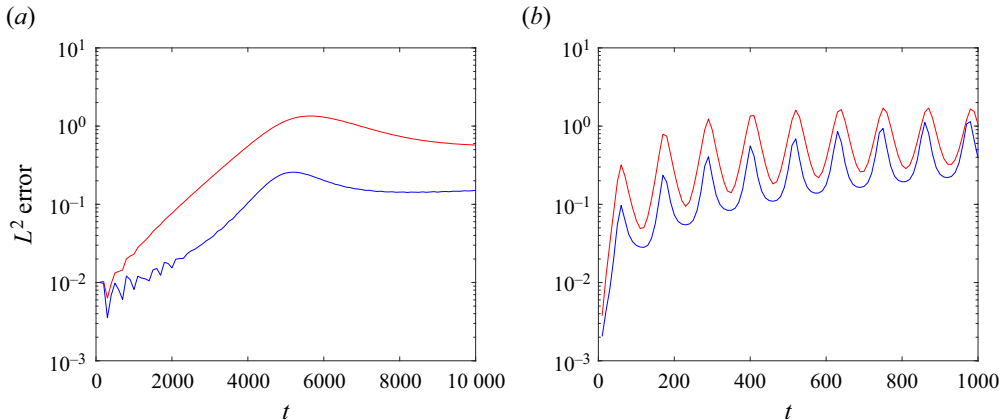


Figure 7. Relative errors on η between fully and weakly nonlinear solutions for $\mathcal{P} = 1$ with (a) $(A_0, k_0, \lambda) = (0.1, 0.9, 0.02)$ and (b) $(A_0, k_0, \lambda) = (0.01, 5, 0.1)$: blue curve, Dysthe equation; red curve, NLS equation.

substantially to the reconstruction process. This result may be attributed to the spectral discretization which limits the possibilities for resonances, or to conditions of the modulational regime being simulated for which quartic resonances are dominant.

Initial conditions of the form

$$u(x, 0) = B_0 [1 + 0.1 \cos(\lambda x)], \quad (7.22)$$

are prescribed for (6.17), where a long-wave perturbation of wavenumber $\lambda \ll k_0$ is superimposed to a uniform solution of amplitude B_0 . For the full system, the initial conditions $\eta(x, 0)$ and $\xi(x, 0)$ are reconstructed by solving (2.8) from transformed initial data (7.7)–(7.8) combined with (7.22). This allows for a meaningful comparison with matching initial conditions. Figure 7 illustrates the time evolution of the relative L^2 errors

$$\frac{\|\eta_f - \eta_w\|_2}{\|\eta_f\|_2}, \quad (7.23)$$

on η between the fully (η_f) and weakly (η_w) nonlinear solutions for $\mathcal{P} = 1$ with $(A_0, k_0, \lambda) = (0.1, 0.9, 0.02)$ and $(0.01, 5, 0.1)$ as considered in the previous stability analysis. The numerical parameters are set to $L = 200\pi$, $N = 1024$ ($\Delta\kappa = 0.01$, $\Delta x = 0.61$), $\Delta t = 0.01$ for $(A_0, k_0, \lambda) = (0.1, 0.9, 0.02)$, and to $L = 20\pi$, $N = 1024$ ($\Delta\kappa = 0.1$, $\Delta x = 0.06$), $\Delta t = 0.0002$ for $(A_0, k_0, \lambda) = (0.01, 5, 0.1)$. As mentioned earlier, a sufficiently long domain is specified in x so that long-wave modulations can be resolved. Needless to say the time scale of these modulations is commensurate with their wavelength. For reference, errors from the cubic NLS equation (by neglecting the higher-order terms in (6.17)) are also shown in this figure. The same reconstruction procedure for η based on (4.20a,b) is adopted in both cases. Overall, L^2 errors from the NLS equation are noticeably higher than those from the Dysthe equation, which confirms the superiority of the latter model in this asymptotic regime. Their values tend to gradually grow over time due to accumulation and amplification of numerical errors during the BF instability process. For $(A_0, k_0, \lambda) = (0.1, 0.9, 0.02)$, these two models differ in performance by almost an order of magnitude. If we switched from $\gamma = 1$ to $\gamma = 2$ for $(A_0, k_0, \lambda) = (0.01, 5, 0.1)$, these curves would be flipped with NLS errors being lower than Dysthe errors. Therefore, figure 7 may serve to validate (5.36) of γ , hence our treatment of cubic resonances.

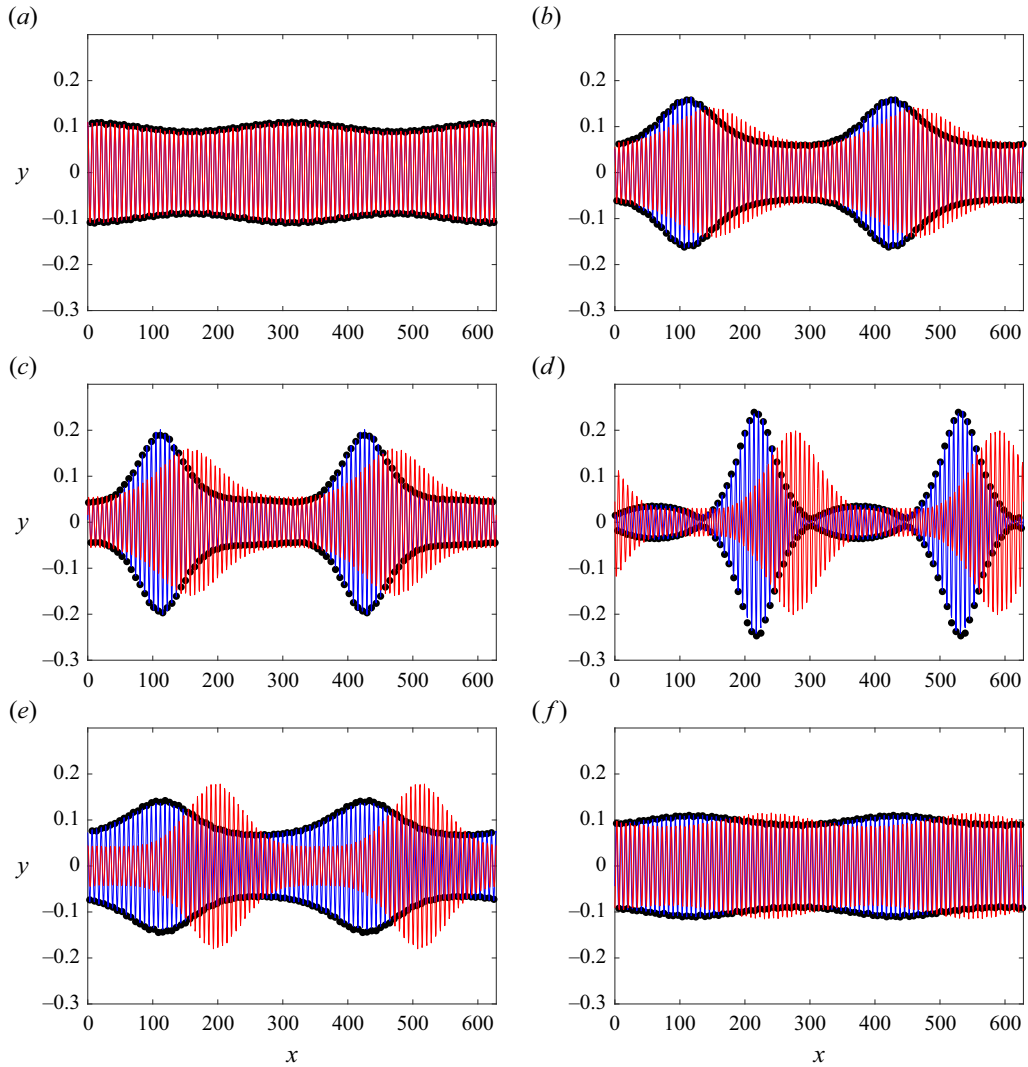


Figure 8. Comparison of η between fully and weakly nonlinear solutions for $(A_0, k_0, \lambda) = (0.1, 0.9, 0.02)$ and $\mathcal{P} = 1$ at (a) $t = 0$, (b) $t = 3400$, (c) $t = 4000$, (d) $t = 5000$, (e) $t = 7000$, (f) $t = 10000$: blue curve, Dysthe equation; red curve, NLS equation; black dots, Euler system.

A comparison of surface profiles η obtained from these two models and the full nonlinear (Euler) system is presented in figures 8 and 9 with snapshots at various instants for $\mathcal{P} = 1$. Again, the two configurations $(A_0, k_0, \lambda) = (0.1, 0.9, 0.02)$ and $(0.01, 5, 0.1)$ are examined. Due to the large aspect ratio and the presence of short oscillations, we simply plot the local maxima (i.e. crests) and local minima (i.e. troughs) of the Euler solution by using dots, without showing its entire profile to avoid cluttering these graphs. Development of the BF instability and associated near-recurrence over time are clearly observed. The snapshots at $t = 5000$ (figure 8) and at $t = 170$ (figure 9) correspond to a time of maximum wave growth with modes $\lambda = 0.02$ (two humps $|p| = 2$) and $\lambda = 0.1$ (a single hump $|p| = 1$) being amplified, respectively, which is consistent with the previous stability analysis (see figure 6).

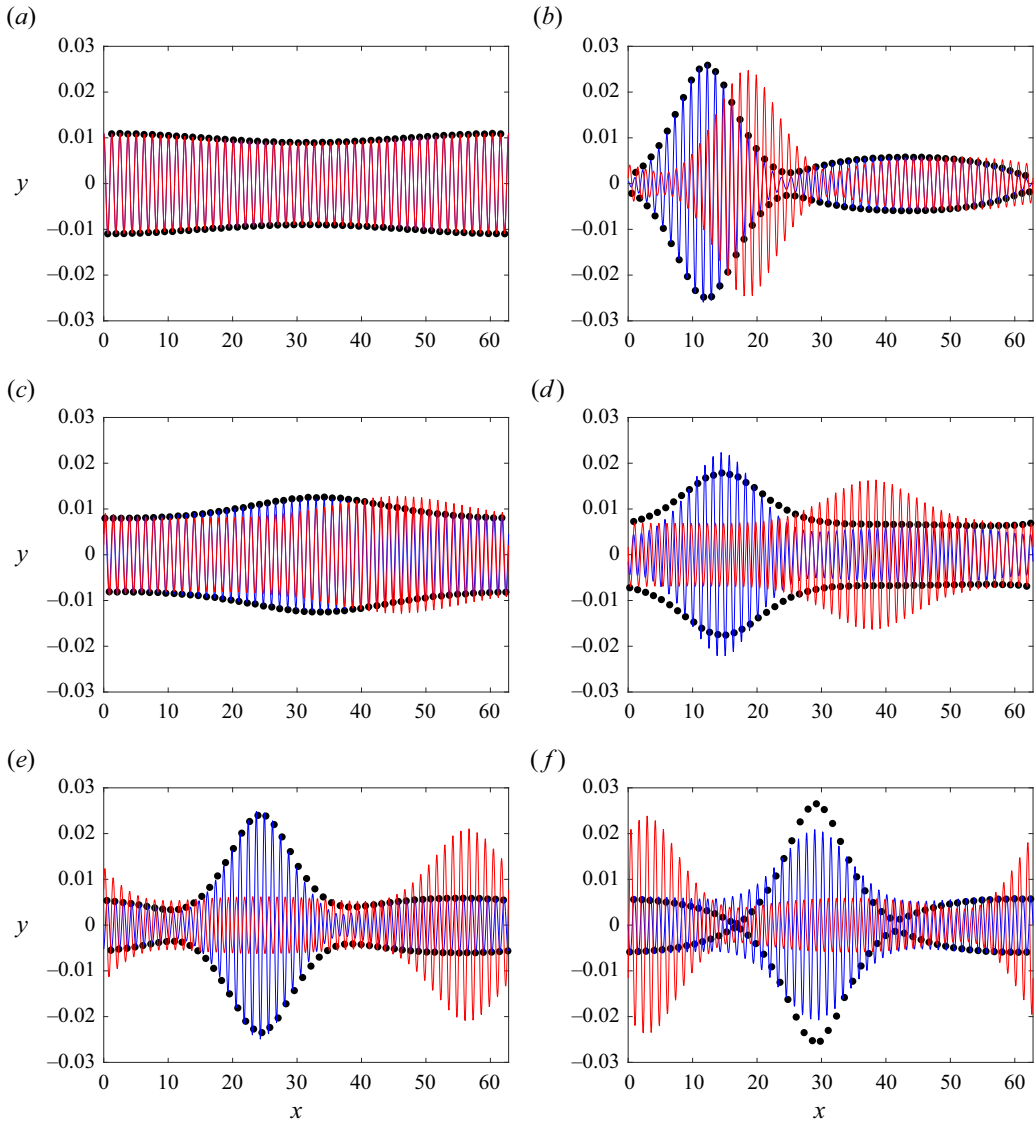


Figure 9. Comparison of η between fully and weakly nonlinear solutions for $(A_0, k_0, \lambda) = (0.01, 5, 0.1)$ and $P = 1$ at (a) $t = 0$, (b) $t = 170$, (c) $t = 320$, (d) $t = 620$, (e) $t = 860$, (f) $t = 980$: blue curve, Dysthe equation; red curve, NLS equation; black dots, Euler system.

Here the waves travel from left to right but, owing to the periodic boundary conditions, they re-enter the domain from one side whenever they exit it through the other side. A striking feature of figure 8 for $(A_0, k_0, \lambda) = (0.1, 0.9, 0.02)$ is the excellent match in phase, amplitude and shape between the Dysthe and Euler solutions throughout the entire simulation. By contrast, the NLS wave packet seems to move faster and the resulting shift accentuates over time. A slight left-right asymmetry is discernible near the tails of the Dysthe and Euler pulses, especially when wave modulation is strong, while such an asymmetry is absent from the NLS pulse. The presence of spatial derivatives of odd order in the Dysthe equation may explain this phenomenon as opposed to the NLS

equation. For $(A_0, k_0, \lambda) = (0.01, 5, 0.1)$, while very good agreement is obtained between the Dysthe and Euler solutions at early stages of their time evolution, discrepancies arise during subsequent cycles of BF instability as shown in [figure 9](#). Notably, the Dysthe wave packet is found to be steeper (respectively, less steep) than the Euler wave packet at $t = 620$ (respectively, $t = 980$), although their phases still match well. In spite of these differences, all three solutions behave qualitatively in the same way during the process of wave modulation–demodulation. These results are in line with the L^2 errors reported in [figure 7](#). Similar observations can be made for other values of $0 \leq \mathcal{P} < 2$ and are not displayed for convenience.

We further assess the performance of our reconstruction procedure by testing it against independent predictions from the NLS equation proposed by Trichtchenko *et al.* (2019) for flexural-gravity waves ($\mathcal{P} = 0$) on deep water. In this framework, the surface variables are determined perturbatively by a Stokes expansion

$$\eta = \eta_1 e^{i\theta} + \eta_2 e^{2i\theta} + \text{c.c.}, \quad Q = \omega_0 \eta_1 e^{i\theta} + 2\omega_0 \eta_2 e^{2i\theta} + \text{c.c.}, \quad (7.24a,b)$$

up to second order, where c.c. denotes complex conjugation, $\theta = k_0 x - \omega_0 t$ and $Q = \partial_x \xi$. The surface velocity potential ξ can be readily deduced from Q as $\xi = \partial_x^{-1} Q$ by using the FFT combined with the zero-mass assumption (to handle indetermination at $k = 0$). The carrier wave envelope η_1 obeys

$$i(\partial_t + \omega'_0 \partial_x) \eta_1 + \frac{\omega''_0}{2} \partial_x^2 \eta_1 + \Gamma |\eta_1|^2 \eta_1 = 0, \quad (7.25)$$

with $\omega_0^2 = gk_0 + k_0^5$ and

$$\omega'_0 = \frac{g + 5k_0^4}{2\omega_0}, \quad \omega''_0 = -\frac{g^2 - 30gk_0^4 - 15k_0^8}{4\omega_0^3}, \quad \Gamma = -\frac{\omega_0 k_0^2 (4g^2 - 27gk_0^4 + 44k_0^8)}{2(g + k_0^4)(g - 14k_0^4)}, \quad (7.26a-c)$$

while the second-harmonic component η_2 is bound to η_1 via

$$\eta_2 = \frac{\omega_0^2 \eta_1^2}{g - 14k_0^4}. \quad (7.27)$$

Recall that the coefficients ω''_0 and Γ for dispersion and nonlinearity coincide with ours in this situation. The NLS equation (7.25) was derived following the method of multiple scales based on an integral reformulation of the Euler system (Trichtchenko *et al.* 2019). The algebraic equations (7.24a,b) to reconstruct (η, ξ) are more explicit and more efficient than (4.20a,b), but they are perturbative and devoid of any Hamiltonian structure. On the other hand, our reconstruction procedure is non-perturbative and involves solving an auxiliary system of Hamiltonian differential equations, as motivated by the basic Hamiltonian formulation of this problem.

Restricting our attention to $\mathcal{P} = 0$, [figure 10](#) compares L^2 errors (7.23) from our NLS equation with (η, ξ) calculated according to (4.20a,b) and from its counterpart (7.25) with (η, ξ) given by (7.24a,b). For each of these models, the L^2 error is estimated relative to the Euler solution with respective initial conditions $\eta(x, 0)$ and $\xi(x, 0)$. In the case where (7.25) is tested against (2.8), these initial conditions are provided by (7.24a,b) and (7.27) with

$$\eta_1(x, 0) = \frac{A_0}{2} [1 + 0.1 \cos(\lambda x)], \quad (7.28)$$

noting again that A_0 and B_0 are related through (7.6) to ensure matching wave parameters between these two NLS models. We adopt the same numerical schemes as described

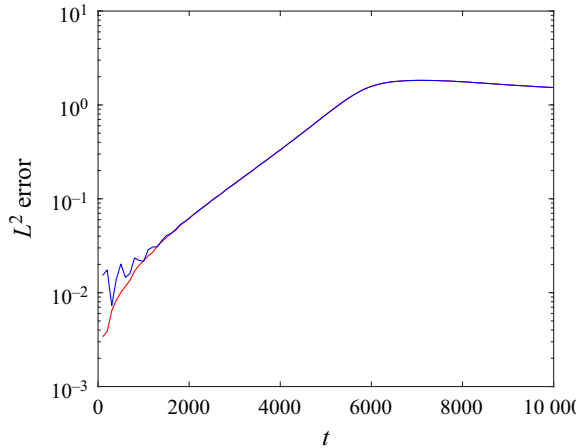


Figure 10. Relative errors on η between fully and weakly nonlinear solutions for $\mathcal{P} = 0$ with $(A_0, k_0, \lambda) = (0.1, 0.9, 0.02)$: blue curve, our NLS equation; red curve, NLS equation from Trichtchenko *et al.* (2019).

earlier, together with the same resolutions in space and time, to solve (7.25) and evaluate (7.24a,b). The initially perturbed Stokes wave is again prescribed by $A_0 = 0.1$, $k_0 = 0.9$ and $\lambda = 0.02$. We find that the two sets of errors are indistinguishable as shown in this figure. This is not surprising given the fact that, for such mild initial conditions and for such a weakly nonlinear solution as produced by the NLS equation, high-order harmonics are not expected to contribute significantly to the wave spectrum. In light of this remarkable agreement, figure 10 helps provide a cross-validation of these two independent methods for reconstructing (η, ξ) from the wave envelope: on one hand, our dynamical system approach based on the numerical solution of (4.20a,b) and, on the other hand, an asymptotic approach based on the second-order algebraic formulae (7.24a,b). Such a validation was not presented by Trichtchenko *et al.* (2019). Finally, the conservation of energy H and wave action M by the Dysthe equation (6.17) is demonstrated in figure 11 where the relative errors

$$\frac{\Delta H}{H_0} = \frac{|H - H_0|}{H_0}, \quad \frac{\Delta M}{M_0} = \frac{|M - M_0|}{M_0}, \quad (7.29a,b)$$

are plotted as functions of time t for $A_0 = 0.1$, $k_0 = 0.9$ and $\lambda = 0.02$. Integration over x in (6.14) and in the L^2 norm (7.23) is carried out via the trapezoidal rule over the periodic domain $[0, L]$. The reference values H_0 and M_0 denote the initial values of (6.14) and (6.19) at $t = 0$. Overall, both H and M are very well conserved by (6.17) for various values of \mathcal{P} . The gradual loss of accuracy over time is likely attributed to accumulation of numerical errors as enhanced by the BF instability.

8. Conclusions

The two-dimensional problem of nonlinear hydroelastic waves propagating along an ice sheet on an ocean of infinite depth is investigated theoretically and computationally. Of interest is the asymptotic modulational regime which is applicable to wave groups as commonly observed under open-water or ice-covered conditions. Based on the Hamiltonian formulation for nonlinear potential flow coupled to a thin-plate representation of the ice cover with nonlinear effects from ice bending and compression, we propose a Hamiltonian version of the Dysthe equation (a higher-order NLS equation) for the

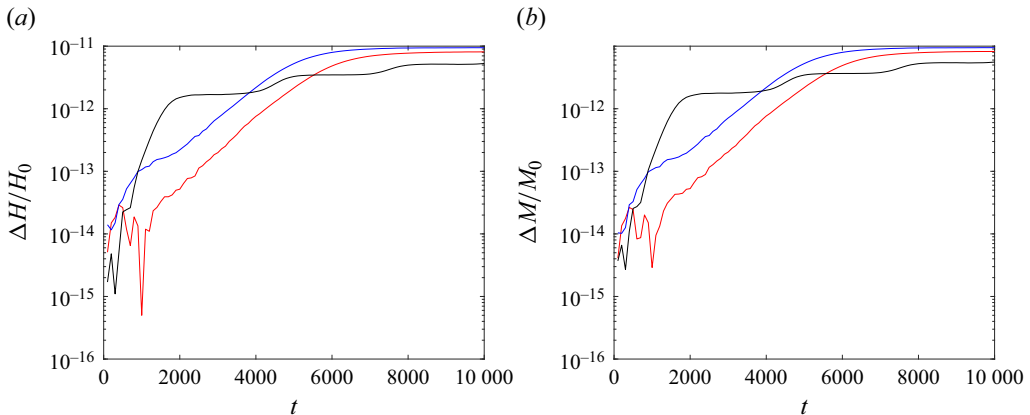


Figure 11. Relative errors on (a) H and (b) M for the Dysthe equation with $(A_0, k_0, \lambda) = (0.1, 0.9, 0.02)$ and $\mathcal{P} = 0$ (red), $\mathcal{P} = 1$ (blue), $\mathcal{P} = 1.9$ (black).

slowly varying envelope of weakly nonlinear quasimonochromatic waves. This model is derived via a systematic approach by applying ideas from Hamiltonian perturbation theory which involve canonical transformations such as reduction to normal form, use of a modulational ansatz and homogenization over short spatial scales. Due to the more complicated dispersion relation (as compared with, for example, the pure gravity case), an additional difficulty here is the presence of resonant triads for which we conduct a detailed examination.

Accordingly, special attention is paid to developing a normal form transformation that eliminates non-resonant triads while accommodating resonant ones. For this purpose, the cubic resonances are identified and treated separately in the Fourier integral terms. This leads to corrections in the normal form transformation as well as in the envelope equation, especially for the mean-flow term. The reduction to normal form is given by an auxiliary system of integrodifferential equations in the Fourier space, and is also endowed with a Hamiltonian structure. Its significance is two-fold as it provides a non-perturbative scheme to reconstruct the ice-sheet deformation from the wave envelope by reversing the evolutionary process. As a consequence, the entire solution (from the envelope equation to the surface reconstruction) fits within a Hamiltonian framework.

Application to the time evolution of perturbed Stokes waves in sea ice is considered. Inspecting first the BF instability criterion for the NLS part of this model, a regime transition from defocusing to focusing occurs when $\mathcal{P} \simeq 0.39$ at k_{min} (at the minimum phase speed), which implies the existence of small-amplitude travelling wave packets. This theoretical result contrasts with previous reports on the non-existence of such solutions (i.e. a defocusing NLS equation at k_{min}) in the absence of ice compression ($\mathcal{P} = 0$). It is supportive of recent observations of persistent wave groups in the Arctic Ocean. This linear stability analysis is then generalized to the higher-order terms for any carrier wavenumber. Its predictions are tested against numerical solutions of the Dysthe equation in the time domain. An assessment in comparison with simulations based on the NLS equation and the full Euler system is also shown. Overall, very good agreement is found, with evidence confirming that the Dysthe equation performs better than the NLS equation. Finally, the proposed scheme for surface reconstruction is verified against independent computations using a more classical approach via a Stokes expansion.

In the future, it would be of interest to carry out a detailed numerical investigation on solitary wave packets of small to large amplitudes over the range $0 \leq \mathcal{P} < 2$, possibly

induced by a moving load along the ice sheet. Another possible extension of this work is to tackle the three-dimensional case where a similar Hamiltonian formulation can be adopted (Guyenne 2015). Furthermore, it is conceivable that the same splitting method can be applied to dealing with cubic resonances in the related problem of gravity-capillary waves.

Funding. Part of this work was carried out when A.K. was a Postdoctoral Fellow at the University of Toronto; A.K. was partially supported by McMaster University, the University of Toronto and Nazarbayev University under grant SPG-064.01.00. P.G. is partially supported by the National Science Foundation (USA) under grant DMS-2307712. P.G. also gratefully acknowledges support by the Japan Society for the Promotion of Science under a short-term Invitational Fellowship for Research in Japan. C.S. is partially supported by the Natural Sciences and Engineering Research Council of Canada (NSERC) under grant RGPIN-2024-03886.

Declaration of interests. The authors report no conflict of interest.

Author ORCIDs.

 Adilbek Kairzhan <https://orcid.org/0009-0005-3442-6629>.

Appendix A. Useful identities

Here we provide a list of identities commonly used in this manuscript.

A.1. Expansions

Below, we list a number of expansion identities that we rely on during the approximation procedure. We do not give any proofs as the derivations are straightforward. Under the modulational regime (5.18), we have the following formulae:

$$\left. \begin{aligned} |k| &= k_0 + \varepsilon \lambda + O(\varepsilon^2), \\ \operatorname{sgn}(k) &= 1, \\ a(k) &= \sqrt{\frac{\omega_0}{k_0}} \left(1 - \frac{\varepsilon \lambda}{4\omega_0^2} \left(g + \mathcal{P}k_0^2 - 3\mathcal{D}k_0^4 \right) \right) + O(\varepsilon^2), \\ \omega(k) &= \omega_0 \left(1 + \frac{\varepsilon \lambda}{2\omega_0^2} \left(g - 3\mathcal{P}k_0^2 + 5\mathcal{D}k_0^4 \right) \right) + O(\varepsilon^2), \\ k_1 - k_3 &= \varepsilon(\lambda_1 - \lambda_3), \\ a_{1-3} &= a(k_1 - k_3) = \frac{g^{1/4}}{\varepsilon^{1/4} |\lambda_1 - \lambda_3|^{1/4}} \left(1 - \frac{\mathcal{P}}{4g} \varepsilon^2 |\lambda_1 - \lambda_3|^2 \right) + O(\varepsilon^{7/4}), \\ \omega_{1-3} &= \omega(k_1 - k_3) = g^{1/2} \varepsilon^{1/2} |\lambda_1 - \lambda_3|^{1/2} \left(1 - \frac{\mathcal{P}}{2g} \varepsilon^2 |\lambda_1 - \lambda_3|^2 \right) + O(\varepsilon^{9/2}). \end{aligned} \right\} \quad (\text{A1})$$

Moreover, we get the following expansions for terms of type $a_{1+2} = a(k_1 + k_2)$ and $\omega_{1+2} = \omega(k_1 + k_2)$:

$$\left. \begin{aligned} a_{1+2} &= \sqrt{\frac{\omega_{2k_0}}{2k_0}} \left(1 - \frac{\varepsilon(\lambda_1 + \lambda_2)}{4\omega_{2k_0}^2} (g + 4\mathcal{P}k_0^2 - 48\mathcal{D}k_0^4) \right) + O(\varepsilon^2), \\ \omega_{1+2} &= \omega_{2k_0} \left(1 + \frac{\varepsilon(\lambda_1 + \lambda_2)}{2\omega_{2k_0}^2} (g - 12\mathcal{P}k_0^2 + 80\mathcal{D}k_0^4) \right) + O(\varepsilon^2). \end{aligned} \right\} \quad (\text{A2})$$

A.2. Integral identities

LEMMA A.1. *Under the modulational ansatz (5.18), given the indices $j, \ell \in \{1, 2, 3, 4\}$ together with $\alpha, \beta \in \{1, 2\}$ and $\mu, \nu \in \{3, 4\}$, we have*

$$\left. \begin{aligned} \int \lambda_j z_1 z_2 \bar{z}_3 \bar{z}_4 \delta_{1+2-3-4} dk_{1234} &= \int \lambda_\ell z_1 z_2 \bar{z}_3 \bar{z}_4 \delta_{1+2-3-4} dk_{1234}, \\ \int |\lambda_\alpha - \lambda_\mu| z_1 z_2 \bar{z}_3 \bar{z}_4 \delta_{1+2-3-4} dk_{1234} &= \int |\lambda_\beta - \lambda_\nu| z_1 z_2 \bar{z}_3 \bar{z}_4 \delta_{1+2-3-4} dk_{1234}. \end{aligned} \right\} \quad (\text{A3})$$

Appendix B. Proof of proposition 5.1

Here we outline the main steps to derive the coefficients in (5.8). For simplicity, we introduce notations I and II to denote the first and second lines of (2.21), respectively, so that $H^{(4)} = I + II$. We rewrite each of I and II in terms of z_k and \bar{z}_{-k} via (2.25).

For I, we have

$$\begin{aligned} I &= \frac{1}{32\pi} \int |k_1||k_4| (|k_1| + |k_4| - 2|k_3 + k_4|) \frac{a_1 a_4}{a_2 a_3} \\ &\quad \times (z_1 - \bar{z}_{-1})(z_2 + \bar{z}_{-2})(z_3 + \bar{z}_{-3})(z_4 - \bar{z}_{-4}) \delta_{1234} dk_{1234} \\ &= \int V_{1234} (z_1 - \bar{z}_{-1})(z_2 + \bar{z}_{-2})(z_3 + \bar{z}_{-3})(z_4 - \bar{z}_{-4}) \delta_{1234} dk_{1234}, \end{aligned} \quad (\text{B1})$$

where we have used the definition (5.9). Extracting terms of type ‘ $zz\bar{z}\bar{z}$ ’, we have

$$\begin{aligned} I_R &= \int V_{1234} (-z_1 z_2 \bar{z}_{-3} \bar{z}_{-4} - \bar{z}_{-1} \bar{z}_{-2} z_3 z_4 - z_1 \bar{z}_{-2} z_3 \bar{z}_{-4} - \bar{z}_{-1} z_2 \bar{z}_{-3} z_4 + z_1 \bar{z}_{-2} \bar{z}_{-3} z_4 \\ &\quad + \bar{z}_{-1} z_2 z_3 \bar{z}_{-4}) \delta_{1234} dk_{1234}. \end{aligned} \quad (\text{B2})$$

This integral can alternatively be written after index rearrangements as

$$I_R = \int (-V_{1234} - V_{4321} - V_{1324} - V_{4231} + V_{1432} + V_{3214}) z_1 z_2 \bar{z}_{-3} \bar{z}_{-4} \delta_{1234} dk_{1234}. \quad (\text{B3})$$

After reindexing $(k_1, k_2, k_3, k_4) \rightarrow (k_1, k_2, -k_3, -k_4)$, we get

$$\begin{aligned} I_R &= \int [-V_{12(-3)(-4)} - V_{(-4)(-3)21} - V_{1(-3)2(-4)} - V_{(-4)2(-3)1} \\ &\quad + V_{1(-4)(-3)2} + V_{(-3)21(-4)}] z_1 z_2 \bar{z}_3 \bar{z}_4 \delta_{1+2-3-4} dk_{1234}, \end{aligned} \quad (\text{B4})$$

with coefficient equal to $T_0^{(1)}$. The computations for II are similar and involve $T_0^{(2)}$.

Appendix C. Proof of proposition 5.2

Here we outline the main steps to derive the coefficients in (5.10). The terms in $\{K^{(3)}, H_{NoRes}^{(3)}\}$ associated with T_{NoRes} in (5.5) are of the form $zz\bar{z}\bar{z}$. To find these terms, we compute the Poisson bracket $\{K^{(3)}, H_{NoRes}^{(3)}\}$ using the expressions (4.16) for $K^{(3)}$ and $H_{NoRes}^{(3)} = H^{(3)} - H_{Res}^{(3)}$ with $H_{Res}^{(3)}$ given in (4.14). To distinguish between the indices associated with $K^{(3)}$ and $H^{(3)}$, we use $\{1, 2, 3\}$ for $K^{(3)}$ and $\{4, 5, 6\}$ for $H^{(3)}$.

To simplify the computations, we decompose $K^{(3)} = K_0^{(3)} + K_\chi^{(3)}$ with

$$\left. \begin{aligned} K_0^{(3)} &= \frac{1}{8i\sqrt{\pi}} \int S_{123} \left[\frac{z_1 z_2 z_3 - \bar{z}_{-1} \bar{z}_{-2} \bar{z}_{-3}}{\omega_1 + \omega_2 + \omega_3} - 2 \frac{z_1 z_2 \bar{z}_{-3} - \bar{z}_{-1} \bar{z}_{-2} z_3}{\omega_1 + \omega_2 - \omega_3} \right] \delta_{123} dk_{123}, \\ K_\chi^{(3)} &= \frac{1}{8i\sqrt{\pi}} \int B_{123} \frac{z_1 \bar{z}_{-2} z_3 - \bar{z}_{-1} z_2 \bar{z}_{-3}}{\omega_1 - \omega_2 + \omega_3} \delta_{123} dk_{123}, \end{aligned} \right\} \quad (C1)$$

where we have used the definition $B_{123} = S_{123}(1 - \chi_{123})$. Similarly, we decompose $H_{NoRes}^{(3)} = H_{NoRes,0}^{(3)} + H_{NoRes,\chi}^{(3)}$ with

$$\left. \begin{aligned} H_{NoRes,0}^{(3)} &= \frac{1}{8\sqrt{\pi}} \int S_{456} [z_4 z_5 z_6 + \bar{z}_{-4} \bar{z}_{-5} \bar{z}_{-6} - 2(z_4 z_5 \bar{z}_{-6} + \bar{z}_{-4} \bar{z}_{-5} z_6)] \delta_{456} dk_{456}, \\ H_{NoRes,\chi}^{(3)} &= \frac{1}{8\sqrt{\pi}} \int B_{456} (z_4 \bar{z}_{-5} z_6 - \bar{z}_{-4} z_5 \bar{z}_{-6}) \delta_{456} dk_{456}. \end{aligned} \right\} \quad (C2)$$

This allows us to rewrite $\{K^{(3)}, H_{NoRes}^{(3)}\}$ as the sum of Poisson brackets

$$\{K_0^{(3)}, H_{NoRes,0}^{(3)}\} + \{K_0^{(3)}, H_{NoRes,\chi}^{(3)}\} + \{K_\chi^{(3)}, H_{NoRes,0}^{(3)}\} + \{K_\chi^{(3)}, H_{NoRes,\chi}^{(3)}\}. \quad (C3)$$

Then, the first bracket in (C3) implies $T_{NoRes}^{(1)}$, the sum of the two brackets in the middle implies $T_{NoRes}^{(2)}$ and the last bracket gives $T_{NoRes}^{(3)}$. Below we only show the computations for the last bracket in (C3) and verify that it leads to $T_{NoRes}^{(3)}$ in (5.10). The other Poisson brackets can be treated in a similar way.

Using the formula (4.2), we have

$$\begin{aligned} i \{K_\chi^{(3)}, H_{NoRes,\chi}^{(3)}\}_R &= \frac{1}{64\pi i} \left[\int B_{123} B_{456} \frac{1}{\omega_1 - \omega_2 + \omega_3} z_1 z_3 \bar{z}_{-4} \bar{z}_{-6} \delta_{25} \delta_{123} \delta_{456} dk_{123456} \right. \\ &\quad - 4 \int B_{123} B_{456} \frac{1}{\omega_1 - \omega_2 + \omega_3} z_2 \bar{z}_{-3} \bar{z}_{-5} z_6 \delta_{14} \delta_{123} \delta_{456} dk_{123456} \\ &\quad - 4 \int B_{123} B_{456} \frac{1}{\omega_1 - \omega_2 + \omega_3} \bar{z}_{-2} z_3 z_5 \bar{z}_{-6} \delta_{14} \delta_{123} \delta_{456} dk_{123456} \\ &\quad \left. + \int B_{123} B_{456} \frac{1}{\omega_1 - \omega_2 + \omega_3} \bar{z}_{-1} \bar{z}_{-3} z_4 z_6 \delta_{25} \delta_{123} \delta_{456} dk_{123456} \right]. \end{aligned} \quad (C4)$$

The formula above needs some clarifications, since the direct application of (4.2) produces 10 different integrals. However, it turns out that some of these integrals are equivalent after index rearrangements as in the following example:

$$\begin{aligned} &\int B_{123} B_{456} \frac{1}{\omega_1 - \omega_2 + \omega_3} \bar{z}_{-1} z_2 z_4 \bar{z}_{-5} \delta_{14} \delta_{123} \delta_{456} dk_{123456} \\ &= \int B_{123} B_{456} \frac{1}{\omega_1 - \omega_2 + \omega_3} z_2 \bar{z}_{-3} \bar{z}_{-5} z_6 \delta_{14} \delta_{123} \delta_{456} dk_{123456}, \end{aligned} \quad (C5)$$

after rearranging the indices $(1, 2, 3) \rightarrow (3, 2, 1)$ and $(4, 5, 6) \rightarrow (6, 4, 5)$ and using the symmetry $B_{123} = B_{321}$. As a result, there are two groups of four equivalent integrals which produce the coefficient 4 on the right-hand side of (C4).

To write the integrals in (C4) in terms of $z_1 z_2 \bar{z}_3 \bar{z}_4$ as in (5.5), we use an appropriate modification of indices, which we explain now. For the first integral in (C4), we start by integrating over k_2 and k_5 . Using δ_{123} and δ_{456} , this leads to

$$\begin{aligned} & \int B_{123} B_{456} \frac{1}{\omega_1 - \omega_2 + \omega_3} z_1 z_3 \bar{z}_4 \bar{z}_6 \delta_{25} \delta_{123} \delta_{456} dk_{123456} \\ &= \int B_{1(-1-3)3} B_{4(-4-6)6} \frac{1}{\omega_1 - \omega_{1+3} + \omega_3} z_1 z_3 \bar{z}_4 \bar{z}_6 \delta_{1346} dk_{1346}. \end{aligned} \quad (\text{C6})$$

Next we reindex $(k_1, k_3, k_4, k_6) \rightarrow (k_1, k_2, -k_3, -k_4)$ and get

$$\begin{aligned} & \int B_{1(-1-3)3} B_{4(-4-6)6} \frac{1}{\omega_1 - \omega_{1+3} + \omega_3} z_1 z_3 \bar{z}_4 \bar{z}_6 \delta_{1346} dk_{1346} \\ &= \int B_{1(-1-2)2} B_{3(-3-4)4} \frac{1}{\omega_1 - \omega_{1+2} + \omega_2} z_1 z_2 \bar{z}_3 \bar{z}_4 \delta_{1+2-3-4} dk_{1234}, \end{aligned} \quad (\text{C7})$$

where we have used the symmetry $B_{(-3)(3+4)(-4)} = B_{(3)(-3-4)(4)}$ and $\delta_{1+2-3-4} = \delta(k_1 + k_2 - k_3 - k_4)$. The resulting coefficient

$$B_{1(-1-2)2} B_{3(-3-4)4} \frac{1}{\omega_1 - \omega_{1+2} + \omega_2}, \quad (\text{C8})$$

corresponds to the first term on the first line of the expression for $T_{\text{NoRes}}^{(3)}$ in (5.12). The other integrals in (C4) are treated in a similar way.

Appendix D. Proof of lemma 5.5

Below we provide an outline of the computational steps that lead to expressions (5.28), (5.29) and (5.30).

Proof of (5.28). First, we note that the terms $S_{(-1-2)12}$, $S_{12(-1-2)}$, $S_{(-3-4)34}$ and $S_{34(-3-4)}$ in the expressions (5.10)–(5.12) vanish. This can be shown by expanding these terms under the modulational ansatz in view of identities in Appendix A. For example, for $k_1 = k_0 + \varepsilon \lambda_1$ and $k_2 = k_0 + \varepsilon \lambda_2$, one can see that

$$1 + \text{sgn}(-k_1 - k_2) \text{sgn}(k_2) = 0, \quad (\text{D1})$$

which is sufficient to verify that $S_{(-1-2)12} = 0$. As a result, we rewrite $T_{\text{NoRes}}^{(1)}$ as

$$\begin{aligned} T_{\text{NoRes}}^{(1)} &= \frac{1}{64\pi} S_{2(-1-2)1} S_{4(-3-4)3} \left(\frac{1}{\omega_1 + \omega_2 + \omega_{1+2}} + \frac{1}{\omega_3 + \omega_4 + \omega_{3+4}} \right) \\ &+ \frac{1}{16\pi} S_{(3-1)(-3)1} S_{(4-2)2(-4)} \left(\frac{1}{\omega_{3-1} + \omega_3 - \omega_1} + \frac{1}{\omega_{4-2} + \omega_2 - \omega_4} \right). \end{aligned} \quad (\text{D2})$$

Using the expansions (A1)–(A2) together with the definitions (4.15) and (5.13), we get for $S_{2(-1-2)1}$, $S_{(3-1)(-3)1}$ the following expressions:

$$\begin{aligned} S_{2(-1-2)1} &= S(k_2, -k_1 - k_2, k_1), \\ &= \omega_0 k_0 \sqrt{\frac{2k_0}{\omega_{2k_0}}} \left(1 + \frac{\varepsilon(\lambda_1 + \lambda_2)}{4} \left(\frac{4}{k_0} + \frac{g + 4\mathcal{P}k_0^2 - 48\mathcal{D}k_0^4}{\omega_{2k_0}^2} \right. \right. \\ &\quad \left. \left. - \frac{g + \mathcal{P}k_0^2 - 3\mathcal{D}k_0^4}{\omega_0^2} \right) \right) \end{aligned} \quad (\text{D3})$$

and

$$S_{(3-1)(-3)1} = k_0 g^{1/4} \varepsilon^{3/4} (1 + \operatorname{sgn}(\lambda_3 - \lambda_1)) |\lambda_3 - \lambda_1|^{3/4}. \quad (\text{D4})$$

Performing similar computations on the remaining terms in (D2), its first line becomes

$$\begin{aligned} & \frac{1}{64\pi} S_{2(-1-2)1} S_{4(-3-4)3} \left(\frac{1}{\omega_1 + \omega_2 + \omega_{1+2}} + \frac{1}{\omega_3 + \omega_4 + \omega_{3+4}} \right) \\ &= c_1^l + \frac{1}{2} c_1^r \varepsilon (\lambda_1 + \lambda_2 + \lambda_3 + \lambda_4), \end{aligned} \quad (\text{D5})$$

while the second line of (D2) is equivalent to

$$\begin{aligned} & \frac{1}{16\pi} S_{(3-1)(-3)1} S_{(4-2)2(-4)} \left(\frac{1}{\omega_{3-1} + \omega_3 - \omega_1} + \frac{1}{\omega_{4-2} + \omega_2 - \omega_4} \right) \\ &= \frac{\varepsilon k_0^2}{4\pi} (1 + \operatorname{sgn}(\lambda_3 - \lambda_1)) |\lambda_3 - \lambda_1|. \end{aligned} \quad (\text{D6})$$

In view of (5.21) and Lemma A.1, this leads to (5.28).

Proof of (5.29). Similarly, noting additionally that $S_{(-3)(3-1)1}$ and $S_{2(4-2)(-4)}$ vanish, the term $T_{\text{NoRes}}^{(2)}$ reduces to

$$\begin{aligned} T_{\text{NoRes}}^{(2)} &= -\frac{1}{16\pi} B_{(4-2)(-4)2} S_{(3-1)(-3)1} \left(\frac{1}{\omega_{3-1} + \omega_3 - \omega_1} + \frac{1}{\omega_{4-2} + \omega_2 - \omega_4} \right) \\ &\quad - \frac{1}{16\pi} B_{(3-1)1(-3)} S_{(4-2)2(-4)} \left(\frac{1}{\omega_{3-1} + \omega_3 - \omega_1} + \frac{1}{\omega_{4-2} + \omega_2 - \omega_4} \right). \end{aligned} \quad (\text{D7})$$

Due to the presence of $\delta_{1+2-3-4}$ inside the right-hand side integral in (5.29), we will see that the leading terms of $T_{\text{NoRes}}^{(2)}$ in (D7) are zero. Indeed, from the definitions of S_{123} and B_{123} , the first line in (D7) contains the factor $B_{(4-2)(-4)2} S_{(3-1)(-3)1}$ involving

$$(1 + \operatorname{sgn}(k_4 - k_2) \operatorname{sgn}(k_2)) (1 + \operatorname{sgn}(k_3 - k_1) \operatorname{sgn}(k_1)). \quad (\text{D8})$$

From the constraint $k_1 + k_2 - k_3 - k_4 = 0$, we have

$$k_1 - k_3 = k_4 - k_2 \implies \operatorname{sgn}(k_3 - k_1) = -\operatorname{sgn}(k_4 - k_2). \quad (\text{D9})$$

Since, under the modulational regime (5.18), $\operatorname{sgn}(k_1) = \operatorname{sgn}(k_2) = +1$, direct computations show that the expression (D8) vanishes, and so does the first line in (D7).

We follow similar steps for the leading term on the second line of (D7). The factor $B_{(3-1)1(-3)} S_{(4-2)2(-4)}$ involves

$$(1 + \operatorname{sgn}(k_3 - k_1) \operatorname{sgn}(-k_3)) (1 + \operatorname{sgn}(k_4 - k_2) \operatorname{sgn}(-k_4)), \quad (\text{D10})$$

which vanishes under the constraint $k_1 + k_2 - k_3 - k_4 = 0$. This leads to (5.29).

Proof of (5.30). The computations for $T_{\text{NoRes}}^{(3)}$ show the effect of resonances in our problem on the coefficients of the quartic Hamiltonian.

Recall the definition $B_{123} = (1 - \chi_{\mathcal{N}_\mu}(k_1, k_2, k_3))S_{123}$. Then, using expansions as in (D3), the first line of (5.12) becomes

$$\begin{aligned} & -\frac{1}{64\pi} B_{1(-1-2)2} B_{3(-3-4)4} \left(\frac{1}{\omega_1 + \omega_2 - \omega_{1+2}} + \frac{1}{\omega_3 + \omega_4 - \omega_{3+4}} \right) \\ & = (1 - \chi_{\mathcal{N}_\mu}(k_1, -k_1 - k_2, k_2))(1 - \chi_{\mathcal{N}_\mu}(k_3, -k_3 - k_4, k_4)) \\ & \quad \times \left(c_2^l + \frac{1}{2} c_2^r \varepsilon (\lambda_1 + \lambda_2 + \lambda_3 + \lambda_4) \right). \end{aligned} \quad (\text{D11})$$

For the second line in (5.12), we perform computations similar to (D6), and obtain that it is equal to

$$\begin{aligned} & \frac{1}{16\pi} B_{(3-1)1(-3)} B_{(4-2)(-4)2} \left(\frac{1}{\omega_{3-1} + \omega_3 - \omega_1} + \frac{1}{\omega_{4-2} + \omega_2 - \omega_4} \right) \\ & = (1 - \chi_{\mathcal{N}_\mu}(k_3 - k_1, k_1, -k_3))(1 - \chi_{\mathcal{N}_\mu}(k_4 - k_2, -k_4, k_2)) \\ & \quad \times \frac{\varepsilon k_0^2}{4\pi} (1 + \text{sgn}(\lambda_1 - \lambda_3)) |\lambda_1 - \lambda_3|. \end{aligned} \quad (\text{D12})$$

Appendix E. Proof of lemma 5.6

The computational steps are similar to those in the proof of lemma 5.5, and we give an outline of these steps below.

For $T_{\text{Res}}^{(1)}$ in (5.14), the first line can be neglected due to the presence of $S_{12(-1-2)}$ and $S_{34(-3-4)}$, both of which vanish due to the presence of a factor of type (D1). For the second line, we also have $S_{(-3)(3-1)1} = 0$ and it reduces to

$$-\frac{1}{16\pi(\omega_{3-1} + \omega_3 - \omega_1)} S_{(3-1)(-3)1} [\chi S]_{(4-2)(-4)2}, \quad (\text{E1})$$

which has a factor given by (D8) vanishing under the assumption $k_1 + k_2 - k_3 - k_4 = 0$. The third line of (5.14) is treated similarly.

For $T_{\text{Res}}^{(2)}$, we follow the steps used in the proof of lemma 5.5. As a result, we get

$$\begin{aligned} & \frac{B_{(3-1)1(-3)}}{\omega_{3-1} + \omega_3 - \omega_1} [\chi S]_{(4-2)(-4)2} = 2\varepsilon k_0^2 (1 - \chi_{\mathcal{N}_\mu}(k_3 - k_1, k_1, -k_3)) \\ & \quad \times \chi_{\mathcal{N}_\mu}(k_4 - k_2, -k_4, k_2) (1 + \text{sgn}(\lambda_1 - \lambda_3)) |\lambda_1 - \lambda_3|. \end{aligned} \quad (\text{E2})$$

Combining this expression with a similar one for the second term on the first line of (5.15), we obtain the first integral contribution to (5.32) under (5.21). Repeating the computation as in (D3) for the terms on the second line of (5.15), we get

$$\begin{aligned} & -\frac{1}{64\pi} \left(\frac{B_{1(-1-2)2}}{\omega_1 + \omega_2 - \omega_{1+2}} [\chi S]_{3(-3-4)4} + \frac{B_{3(-3-4)4}}{\omega_3 + \omega_4 - \omega_{3+4}} [\chi S]_{1(-1-2)2} \right) \\ & = \frac{1}{2} [\chi_{\mathcal{N}_\mu}(k_1, -k_1 - k_2, k_2) + \chi_{\mathcal{N}_\mu}(k_3, -k_3 - k_4, k_4) \\ & \quad - 2\chi_{\mathcal{N}_\mu}(k_1, -k_1 - k_2, k_2)\chi_{\mathcal{N}_\mu}(k_3, -k_3 - k_4, k_4)] \left(c_2^l + \varepsilon c_2^r (\lambda_2 + \lambda_3) \right), \end{aligned} \quad (\text{E3})$$

which yields the second integral contribution to (5.32).

REFERENCES

AKYLAS, T.R. 1983 Envelope solitons with stationary crests. *Phys. Fluids A* **5**, 789–791.

ALBERELLO, A. & PÁRÁU, E.I. 2022 A dissipative nonlinear Schrödinger model for wave propagation in the marginal ice zone. *Phys. Fluids* **34**, 061702.

ALBERELLO, A., PÁRÁU, E.I. & CHABCHOUB, A. 2023 The dynamics of unstable waves in sea ice. *Sci. Rep.* **13**, 13654.

CHEN, H., GILBERT, R.P. & GUYENNE, P. 2019 Dispersion and attenuation in a porous viscoelastic model for gravity waves on an ice-covered ocean. *Eur. J. Mech. (B/Fluids)* **78**, 88–105.

COIFMAN, R. & MEYER, Y. 1985 Nonlinear harmonic analysis and analytic dependence. *Proc. Symp. Pure Maths* **43**, 71–78.

COLLINS III, C.O., ROGERS, W.E., MARCENKO, A. & BABANIN, A.V. 2015 In situ measurements of an energetic wave event in the Arctic marginal ice zone. *Geophys. Res. Lett.* **42**, 1863–1870.

CRAIG, W., GUYENNE, P. & SULEM, C. 2010 A Hamiltonian approach to nonlinear modulation of surface water waves. *Wave Motion* **47**, 552–563.

CRAIG, W., GUYENNE, P. & SULEM, C. 2021a Normal form transformations and Dysthe's equation for the nonlinear modulation of deep-water gravity waves. *Water Waves* **3**, 127–152.

CRAIG, W., GUYENNE, P. & SULEM, C. 2021b The water wave problem and Hamiltonian transformation theory. In *Waves in Flows* (ed. T. Bodnár, G. Galdi & Š. Nečasov), *Advances in Mathematical Fluid Mechanics*, pp. 113–196. Birkhäuser.

CRAIG, W. & SULEM, C. 1993 Numerical simulations of gravity waves. *J. Comput. Phys.* **108**, 73–83.

CRAIG, W. & SULEM, C. 2016 Mapping properties of normal forms transformations for water waves. *Boll. Unione Mat. Ital.* **9**, 289–318.

DINVAY, E., KALISCH, H. & PÁRÁU, E.I. 2019 Fully dispersive models for moving loads on ice sheets. *J. Fluid Mech.* **876**, 122–149.

DYSTHE, K.B. 1979 Note on a modification to the nonlinear Schrödinger equation for application to deep water waves. *Proc. R. Soc. Lond. A* **369**, 105–114.

GEMMRICH, J., MUDGE, T. & THOMSON, J. 2021 Long-term observations of the group structure of surface waves in ice. *Ocean Dyn.* **71**, 343–356.

GUYENNE, P. 2015 Envelope equations for three-dimensional gravity and flexural-gravity waves based on a Hamiltonian approach. *Fields Inst. Commun.* **75**, 135–161.

GUYENNE, P., KAIRZHAN, A. & SULEM, C. 2022a Hamiltonian Dysthe equation for three-dimensional deep-water gravity waves. *Multiscale Model. Simul.* **20**, 349–378.

GUYENNE, P., KAIRZHAN, A. & SULEM, C. 2022b A Hamiltonian Dysthe equation for deep-water gravity waves with constant vorticity. *J. Fluid Mech.* **949**, A50.

GUYENNE, P., KAIRZHAN, A., SULEM, C. & XU, B. 2021 Spatial form of a Hamiltonian Dysthe equation for deep-water gravity waves. *Fluids* **6**, 103.

GUYENNE, P. & PÁRÁU, E.I. 2012 Computations of fully nonlinear hydroelastic solitary waves on deep water. *J. Fluid Mech.* **713**, 307–329.

GUYENNE, P. & PÁRÁU, E.I. 2014 Finite-depth effects on solitary waves in a floating ice sheet. *J. Fluids Struct.* **49**, 242–262.

GUYENNE, P. & PÁRÁU, E.I. 2017 Numerical simulation of solitary-wave scattering and damping in fragmented sea ice. In *Proceedings of the 27th International Ocean Polar Engineering Conference, San Francisco, USA, June 25–30* (ed. D. Angelides, R. Ayer, J.S. Chung, R.H. Knapp & H. Park), pp. 373–380. ISOPE.

HARTMANN, M.C.N., VON BOCK UND POLACH, F., EHLERS, S., HOFFMANN, N., ONORATO, M. & KLEIN, M. 2020 Investigation of nonlinear wave-ice interaction using parameter study and numerical simulation. *J. Offshore Mech. Arctic Engng* **142**, 021601.

HOGAN, S.J. 1985 The fourth-order evolution equation for deep-water gravity-capillary waves. *Proc. R. Soc. Lond. A* **402**, 359–372.

LIU, A.K. & MOLLO-CHRISTENSEN, E. 1988 Wave propagation in a solid ice pack. *J. Phys. Oceanogr.* **18**, 1702–1712.

MARCENKO, A.V. & SHRIRA, V.I. 1992 Theory of two-dimensional nonlinear waves in liquid covered by ice. *Fluid Dyn.* **26**, 580–587.

MARKO, J.R. 2003 Observations and analyses of an intense waves-in-ice event in the Sea of Okhotsk. *J. Geophys. Res.* **108**, 3296.

MLEWSKI, P., VANDEN-BROECK, J.-M. & WANG, Z. 2011 Hydroelastic solitary waves in deep water. *J. Fluid Mech.* **679**, 628–640.

MLEWSKI, P. & WANG, Z. 2013 Three dimensional flexural-gravity waves. *Stud. Appl. Maths* **131**, 135–148.

PĀRĀU, E.I. & DIAS, F. 2002 Nonlinear effects in the response of a floating ice plate to a moving load. *J. Fluid Mech.* **460**, 281–305.

PLOTNIKOV, P.I. & TOLAND, J.F. 2011 Modelling nonlinear hydroelastic waves. *Phil. Trans. R. Soc. Lond. A* **369**, 2942–2956.

SCHULKES, R.M.S.M., HOSKING, R.J. & SNEYD, A.D. 1987 Waves due to a steadily moving source on a floating ice plate. Part 2. *J. Fluid Mech.* **180**, 297–318.

SLUNYAEV, A.V. & STEPANYANTS, Y.A. 2022 Modulation property of flexural-gravity waves on a water surface covered by a compressed ice sheet. *Phys. Fluids* **34**, 077121.

SLUNYAEV, A.V. & STEPANYANTS, Y.A. 2024 Frequency downshifting in decaying wavetrains on the ocean surface covered by ice floes. *Phys. Fluids* **36**, 036621.

SQUIRE, V.A. 2020 Ocean wave interactions with sea ice: a reappraisal. *Annu. Rev. Fluid Mech.* **52**, 7–60.

TAKIZAWA, T. 1985 Deflection of a floating sea ice sheet induced by a moving load. *Cold Reg. Sci. Technol.* **11**, 171–180.

TRICHTCHENKO, O., MILEWSKI, P., PĀRĀU, E. & VANDEN-BROECK, J.-M. 2019 Stability of periodic traveling flexural-gravity waves in two dimensions. *Stud. Appl. Maths* **142**, 65–90.

XU, B. & GUYENNE, P. 2023 Nonlinear simulation of wave group attenuation due to scattering in broken floe fields. *Ocean Model.* **181**, 102139.

XU, L. & GUYENNE, P. 2009 Numerical simulations of three-dimensional nonlinear water waves. *J. Comput. Phys.* **228**, 8446–8466.

ZAKHAROV, V.E. 1968 Stability of periodic waves of finite amplitude on the surface of a deep fluid. *J. Appl. Mech. Tech. Phys.* **9**, 190–194.